Aus der Klinik für Radiologie
der Medizinischen Fakultät Charité – Universitätsmedizin Berlin

DISSERTATION

The Diagnostic Potential of Metabolomic Prostate Cancer Field Effects

zur Erlangung des akademischen Grades
Doctor medicinae (Dr. med.)

vorgelegt der Medizinischen Fakultät
Charité – Universitätsmedizin Berlin

von

Sarah Svenja Dinges

Datum der Promotion: 26.06.2022

Inhaltsverzeichnis

Abbildungsverzeichnis

Abkürzungsverzeichnis

1H HRMAS	Proton high-resolution magic angle spinning
Ala	Alanine
ANOVA	Analysis of variance
ATP	Adenosine triphosphate
AUROC	Area under the receiver operating characteristic
BCR	Biochemical recurrence
Ca	Tissue sample, histologically cancer
Cho	Choline
choCC	Choline containing compounds and choline
COSMOS	Coordination of Standards in Metabolomics
Crea	Creatine
DRE	Digital rectal examination
EV	Eigenvalue
FA	Fatty acids
FDG-PET	18F-fluorodeoxyglucose positron emission tomography
Fig.	Figure
GS	Gleason Score
Hb	Histologically benign
HbA	Tissue sample, histologically benign adjacent to cancer (distance ≤5 mm)
HbABC	Tissue samples, HbA, HbB and HbC grouped
HbB	Tissue sample, histologically benign adjacent to cancer (distance ≤10 mm, >5 mm)
HbBC	Tissue samples, HbB and HbC grouped
HbC	Tissue sample, histologically benign adjacent to cancer (distance >10 mm)
HMDB	Human Metabolome Database
KEGG	Kyoto Encyclopedia of Genes and Genomes
MGH	Massachusetts General Hospital
(mp)MRI	(Multiparametric) Magnetic Resonance Imaging
MRS	Magnetic Resonance Spectroscopy
MS	Mass Spectroscopy
NAA	N-acetylaspartate
PCA, PC	Principal component analysis, principal component

PCPGG	Prostate cancer prognostic grade groups
PET	Positron emission tomography
PhCrea	Phosphocreatine
PhoCho	Phosphatidylcholine
PLS-DA	Partial least squares discriminant analysis
ppm	Parts per million
PSA	Prostate specific antigen
ROC	Receiver operating characteristic
ROI	Region of interest
Succ-CoA	Succinyl-coenzyme A
TCA	Tricarboxylic acid cycle
TRUS	Transrectal ultrasound
USA	United States of America
VIP	Variable Importance in the Projection
Vol%	Volume percentage of the tissue components stroma, glands or cancer
vs.	versus
ZIP1	Zinc transporter 1
α-KG	α-ketoglutarate

Abstract (Deutsch)

Beim Prostatakarzinom, der häufigsten Krebserkrankung des Mannes, kann die Bedeutung präziser Diagnosestellung und Risikoabschätzung kaum überschätzt werden. Der Verlauf der Erkankung variiert von ungefährlich bis hochaggressiv, dementsprechend unterscheiden sich auch die jeweiligen therapeutischen Ansätze. Deshalb ist es ein Problem, dass Prostatabiopsien derzeit hohe Raten an falsch-negativen Befunden oder fehleingeschätzter Aggressivität liefern. Verbesserungsmöglichkeiten bieten metabolomische Daten, insbesondere aus histologisch benignem Prostatagewebe. In der vorliegenden Arbeit untersuchen wir erstmalig an ganzen Organen, ob metabolomische Profile aus histologisch benignem Gewebe über den Abstand zu einem benachbarten Krebsherd und dessen Ausmaß und Aggressivität informieren können.

Spektroskopische Daten aus je sechzehn Gewebeproben aus zehn mittels Radiakale Prostatektomie gewonnenen Organen wurden mittels protonenbasierter, hochauflösender sogenannter *magic angle spinning* Magnetresonanzspektroskopie erhoben. Anschließend wurden diese Gewebeproben sowie das verbleibende Gewebe der Organe histologisch begutachtet. Dann wurden die Organe virtuell dreidimensional rekonstruiert. Univariate und multivariate Analysen, letztere mit und ohne Überwachung, ergaben signifikante Unterschiede der metabolomische Profile histologisch benigner (Hb) Gewebeproben aus verschiedenen Abständen zu einem Krebsherd (HbA, ≤ 5 mm, n=124; HbB, > 5 mm, ≤10 mm, n=6; HbC, >10 mm, n=4). Dazu trugen maßgeblich die Metabolite Myo-Inositol, Cholin, Cholin-enthaltende Moleküle und Lipide bei. Signifikant unterschiedlich waren auch metabolomische Profile aus der Nachbarschaft von Krebs mit unterschiedlichem Gleason Score (GS) (≤ 3+4, HbA n=60, HbB und HbC n=7; ≥ 4+3, HbA n=60, HbB und HbC n=3), allerdings lediglich bei kleinem Abstand zum Krebsherd (≤ 5 mm). Maßgeblich trugen Myo-Inositol, Polyamine und Zitrat zu den Unterschieden bei. Auch unterschieden sich metabolomische Profile aus der Nachbarschaft von Krebs unterschiedlicher Größe (klein, HbA n=21; groß, HbA n=99, HbB and HbC n=10) mit den Schlüsselmetaboliten Taurin und Polyamin. Diese Ergebnisse zeigten sich auch innerhalb einzelner Organe. In Analysen, bei denen die Gewebeproben nach ihrem Anteil an Stroma stratifiziert wurden, waren die Unterschiede ebenfalls signifikant, allerdings nur in der Untergrupe mit hohem Stromaanteil (> 80%).

Zusammenfassend haben wir gezeigt, dass metabolomische Profile aus histologisch benignem Prostatagewebe aus unmittelbarer Nähe eines Krebsherdes (1.) je nach GS und räumlichem Ausmaß des Herdes variieren und (2.) sich von Gewebeproben aus größerer Entfernung unterscheiden. Im wissenschaftlichen Bereich lassen diese Ergebnisse die gängige Praxis, histologisch benignes Gewebe von krebsbefallenen Prostatas als bloße “gesunde Kontrolle” zu

verwenden, fragwürdig erscheinen und stellen eine mögliche Erklärung für variierende Ergebnisse bisheriger Studien dar. In der klinischen Anwendung könnten metabolomische Messungen den Zielbereich der Biopsie vergrößern, dadurch das bisherige diagnostische Verfahren ergänzen und die Raten an falsch-negativen Befunden und unterschätzer Aggressivität verkleinern.

Abstract (Englisch)

In prostate cancer, the most frequent malignancy in men, the importance of accurate detection and assessment of aggressiveness cannot be overestimated. The behavior of the disease varies from indolent to fatal, requiring different treatment strategies. However, prostate biopsies have high rates of missed cancers, undergrading and overdiagnosis. Metabolomic data, especially from histologically benign tissue, offer possibilities for improvement. Here, we examine for the first time the potential of spectroscopic data from histologically benign prostate tissue from whole organs to indicate an adjacent cancer´s distance, extent and aggressiveness.

Sixteen samples per organ from ten prostatectomy-removed organs were measured non-destructively with proton high-resolution magic angle spinning magnetic resonance spectroscopy, followed by quantitative histology of the scanned samples and the remaining tissue of the whole organs, and virtual 3D reconstruction of the prostates. Both overall-organ and within-organ, univariate as well as unsupervised and supervised multivariate analysis were applied. Metabolomic profiles in histologically benign (Hb) tissue differed significantly at different distances from the cancer (HbA, ≤ 5 mm, n=124; HbB, > 5 mm, ≤ 10 mm, n=6; HbC, > 10 mm, n=4) with key discriminatory metabolites myo-inositol, choline, choline containing compounds and lipids. Profiles in histologically benign samples adjacent to cancer varied with Gleason Score (GS) (GS $\leq$ 3+4, HbA n=60, HbB and HbC n=7; GS $\geq$ 4+3, HbA n=60, HbB and HbC n=3) and extent (extent less, HbA n=21; extent more, HbA n=99, HbB and HbC n=10) of the adjacent cancer; but, interestingly, at distances > 5 mm these differences disappeared (GS) or were less prominent (extent). Major distinguishing metabolites were myo-inositol, polyamines and citrate for GS and taurine and polyamines for extent. These findings were stable in within-organ analyses and in analyses matched for tissue composition of stroma and glands, but, notably, only in tissue with higher percentages of stroma ($> 80\%$).

Overall, we revealed that metabolomic profiles in histologically benign prostate tissue close to cancer (1) vary with GS and the extent of the cancer and (2) differ from samples at greater distance. These findings challenge the use of histologically benign tissue from cancerous prostates as a mere healthy control, without taking distance to cancer into account, a common practice and possible explanation for varying results in studies. Metabolomic measurements could ultimately complement the current diagnostic procedure, thus enlarging the target area for biopsies into histologically benign environments, and decrease rates of missed cancers, undergrading and overdiagnosis.

1. Introduction

1.1. Prostate cancer diagnosis

Prostate cancer is the most frequently diagnosed malignancy affecting men in Germany, with 58,780 new cases in 2016.[1] The clinical behavior of the disease ranges from indolent, non-invasive tumors to aggressive metastatic cancer with considerable morbidity and mortality, making it the second leading cause of cancer death for men in Germany with 14,417 deaths in 2016.[1,2]

The gold standard for diagnosis is a transrectal ultrasound (TRUS)-guided biopsy. The indications for men aged 45 years or older with a life expectancy of at least ten years comprise an abnormal digital rectal examination (DRE) and repeatedly elevated or rising levels of prostate specific antigen (PSA).[3] Unfortunately, the weak sensitivity and specificity of PSA, DRE and TRUS for detecting cancer lead to high rates of both missed and unnecessary biopsies.[3,4]

A TRUS-guided biopsy encompasses ten to twelve biopsy cores that are taken systematically, with additional cores targeting regions that were identified to be suspicious in the DRE or TRUS.[3] Cancerous tissue samples are graded based on their glandular architecture to give a Gleason Score (GS), which indicates prostate cancer´s aggressiveness. The clinical decisions that follow the diagnosis, ranging from non-invasive monitoring to surgery and radiation, are based on these grades.[2] However, systematic biopsies miss 30% of all cancers and 21% of the clinically significant cancers, defined as high-risk cancers of GS ≥ 4+5.[5,6] Furthermore, as 90% of prostate cancers are multifocal with lesions of varying GS, a biopsy may miss the most aggressive lesion.[7] 20–70% of all cases are thus subject to the under-grading of the GS.[8,9] At the same time, overdiagnosis, the detection of cancer that grows so slowly that death from other causes may precede prostate cancer symptoms, occurs at high rates.[10] While 30 to 70% of men older than 60 years of age have potentially detectable prostate cancer, the lifetime risk of death or metastatic disease is as low as 4%.[11]

For special questions and in the case of re-biopsy, pre-biopsy multiparametric magnetic resonance imaging (mpMRI), which uses multiple MRI sequences conjunctively, and MRI-guided biopsies are recommended.[3] A pre-biopsy mpMRI could reduce potentially unnecessary biopsies by excluding 27% of the men from biopsies, thereby reducing overdiagnosis by 5%.[10] However, due to false negative findings in 11% of cases, a biopsy should be offered anyway.[3] At the same time, the mpMRI, having a specificity of 41%, leads to false positive findings and unnecessary biopsies[3,10] Meanwhile, MRI-targeted biopsies can either be conducted by simply remembering the suspicious locations on mpMRI images during a TRUS-guided biopsy, or in a software-assisted manner by combining mpMRI images with real-time TRUS, or by conducting the biopsy directly within the mpMRI scanner.[4] These three techniques have equal performance in detecting clinically significant cancers.[10,12] The percentage of biopsy cores that are positive for clinically significant cancers increases from 10% in systematic biopsies to 29% in MRI-targeted biopsies.[13] At the same time, overdiagnosed cases are halved.[5] Unfortunately, false negative MRI-targeted biopsies occur in 10% of the cases.[10] As the missed lesions differ from those that are missed in systematic biopsies, a combination of systematic and targeted biopsies can reduce the number of missed cases.[3,14] However even then, false negative cases remain an unsolved problem and the advantage may only be relevant to subgroups, for example, for men with high prostate volumes.[5,15]

Inaccuracies in cancer detection and the assessment of aggressiveness can lead to both underdiagnosis and overdiagnosis. Under-grading correlates with higher rates of extraprostatic tumor extension (22% vs 4%, $p < 0.01$) and relapse (10% vs 3%, $p < 0.01$).[8] Underdiagnosis and under-grading lead to undertreatment and repeated biopsies, with the associated risks. Two percent of men undergoing prostate biopsies experience bleeding, infection, or urinary obstruction and 1% require hospitalization.[16,17] Overdiagnosis, on the other hand, exposes men to the psychological distress of a cancer diagnosis and overtreatment.[18] Even though only 20% of men diagnosed with prostate cancer are high-risk, up to 50% receive intense therapy, such as a radical prostatectomy or radiation therapy, with risk of severe side-effects.[16,19] Underdiagnosis, overdiagnosis, and unnecessary biopsies lead to worse patient outcomes and high public health costs. The lesson learned is that tools for prostate cancer detection and the assessment of aggressiveness cannot be separated from one another as the behavior of the disease and the related clinical decisions vary substantially. Currently, clinical decision-making that meets the needs of each individual patient is not possible. Complementary approaches to gain information about the presence and aggressiveness of prostate cancer are urgently needed.

1.2. Metabolomic prostate cancer biomarkers

The term “metabolomics” translates to small-molecule products of metabolic processes (“metabo-”) that are analyzed holistically as large sets (“-omics”).[20] Metabolites summarize the upstream processes of biological information flow, including genomics and proteomics, and are influenced by the environment. Because they most closely represent biochemical activity and a system’s phenotype, they are attractive for biomarker research.[22] Either untargeted or targeted studies can be conducted. In an untargeted study, as many metabolites as possible are captured simultaneously without prior hypotheses. Subsequent analyses aim to identify a metabolomic profile that characterizes a biological process, for example prostate cancer. Untargeted studies are typically used for biomarker discovery and hypothesis generation and were used in the work presented here. A targeted study, on the contrary, is hypothesis-driven and often used for validation studies looking at a predefined, small set of metabolites.[21,23] For example, sarcosine was first identified as a potential biomarker in tissue for prostate cancer in an untargeted study and then, later on, re-examined by targeted studies.[24,25]

The two main measurement platforms for metabolomic data are mass spectroscopy (MS) and magnetic resonance spectroscopy (MRS). In MS, ionized compounds of samples are separated relative to their mass and characterized by mass-to-charge ratios. This is often preceded by a separation step in liquid or gas chromatography columns. MRS is based on energy absorption and re-emission of atoms in an external magnetic field. Due to its natural abundance, hydrogen is the most widely used nucleus in spectroscopy, followed by phosphorus.[23] Representative MRS spectra are given in Fig. 1.

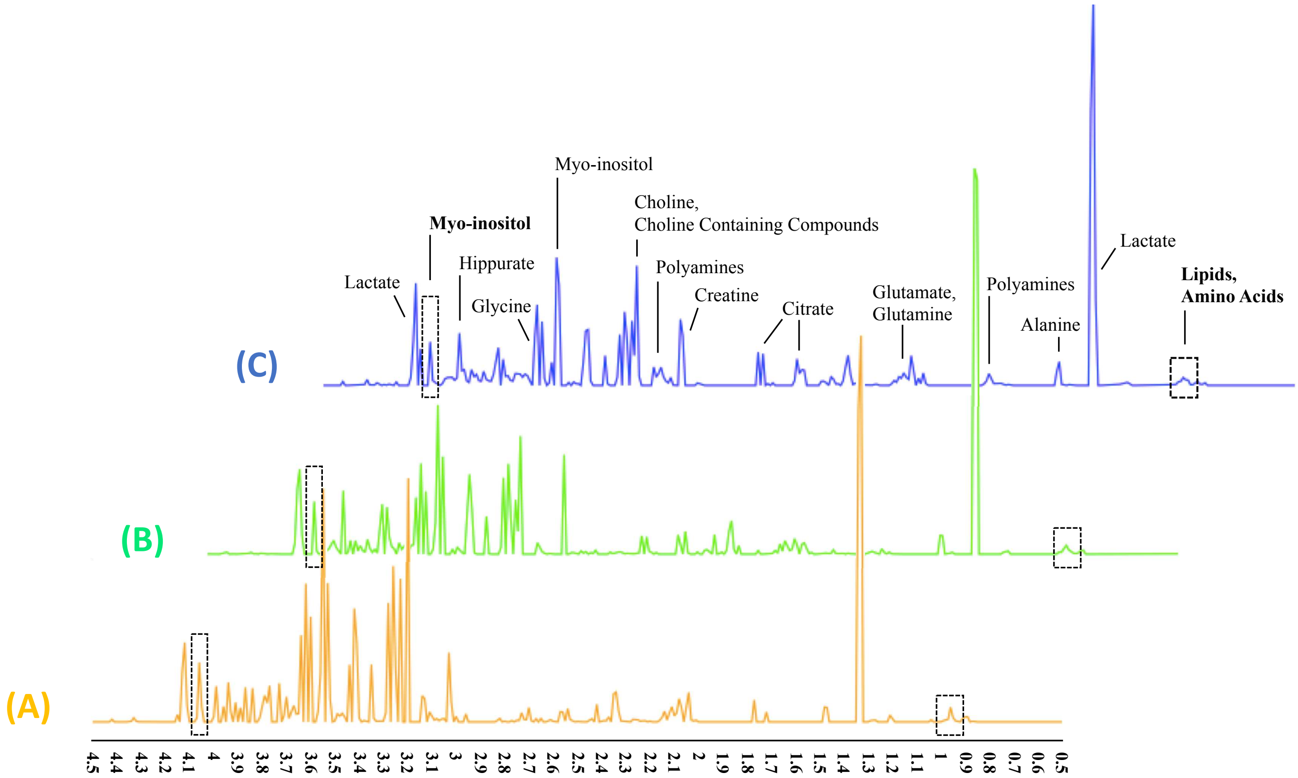

FIGURE 1. Representative one-dimensional MRS spectra of tissue. The position of a peak on the x-axis is called chemical shift and is given in parts per million (ppm). Characteristic peaks are labeled with corresponding metabolites. The y-axis represents the relative concentration. In general, metabolomic studies aim to identify peaks that vary between comparison groups. Here, representative spectra from three tissue samples from one prostate are given. The three samples are histologically benign and have different distances to a nearby cancer lesion: (A) ≤ 5 mm, (B) > 5 mm and ≤10 mm, and (C) > 10 mm. Exemplary peaks that decrease in intensity with increasing distance to cancer ((A) to (B) to (C)) are highlighted in boxes. Figure adapted with permission from REF[26], CC BY 4.0 (https://creativecommons.org/licenses/by/4.0/).

Peak patterns are characteristic for each molecule, as the position on the x-axis depends on the local chemical and magnetic environment of the atom. The position of the peaks is called chemical shift and is given in parts per million (ppm). The ppm value makes spectra obtained at different field strengths comparable. It is calculated as the difference of the resonance frequencies of an added reference compound, typically 3-trimethylsilylpropionate, and the metabolite of interest, divided by the operating frequency. Of note, several metabolites can contribute to one peak, and one metabolite can cause several peaks. The value on the y-axis represents the relative concentration. Absolute concentrations can be measured relative to a reference of known concentration. Two-dimensional MRS can separate overlaps with two spectral axes that display measurements varying in frequencies, nuclei of interest, or different pulse sequences.[23] In comparison with MRS, MS requires only a small amount of the sample. It is less costly and has a sensitivity of two to three orders of magnitude higher compared to MRS, making it superior for targeted studies. However, whereas MS requires technical variations for different metabolites, MRS can simultaneously measure large amounts of metabolites. Also, MRS has a higher reproducibility, requires minimal sample preparation, and can identify previously unknown metabolites by providing information about their chemical structure. Therefore, MRS is preferable for untargeted analysis and was chosen for the study presented here.[21]

Most commonly, metabolomic cancer biomarker studies are conducted in serum, urine, or tissue.[27,28] Studies in serum or urine assume that cancer causes global changes in an organism and compare groups differentiated by patient metadata, e.g. cancer patients vs. healthy controls. In tissue, on the contrary, sample characteristics need to be considered as well. There is for example a difference between cancerous and benign tissue from a cancer patient. Therefore, non-destructive metabolomic measurements that enable subsequent histopathological evaluation are needed.[29] In traditional MRS measurements of liquid samples, the molecules' rapid isotropic motion averages out the anisotropic interactions, leading to high resolution. Previously, the destructive procedure of chemical extraction was needed to obtain an equal resolution in solid tissue.[30] Subsequently, in 1996, the laboratory in which the work presented here was conducted introduced the technique of proton high-resolution magic angle spinning magnetic resonance spectroscopy (^{1}H HRMAS MRS).[31] The intact tissue sample is spun at the so-called magic angle of 54,7° relative to the magnetic field. The spinning frequency in kilohertz exceeds the anisotropic interactions, averages them to their isotropic value, and removes magnetic susceptibility, resulting in highly resolved spectra.[29,32] To date, at least 21 metabolomic tissue studies of prostate cancer have been published.[27] Metabolomics can successfully distinguish cancerous from healthy prostate tissue.[32–42] Measurements in cancer tissue samples were correlated successfully with PSA,[32,40] prostate volume,[40] features of prostate biopsies (GS, benign prostatic hyperplasia, inflammation, and percentage of cancer in a biopsy core)[32–34,38–42], pTNM stages,[32,38–40,43] and biochemical recurrence

(BCR).[34,40,44] Histologically benign tissue from cancerous prostates is mostly used as mere control group with no subgroup analysis within the benign samples.[24,25,34,36,40,41]

1.3. Metabolomics in histologically benign prostate tissue adjacent to cancer

In 1953, Slaughter described “histologically abnormal tissue surrounding cancerous lesions.” He named this phenomenon “field cancerization” because it occurred in an entire *field* of tissue. For him, this phenomenon was the reason for multifocality and local recurrence of oral squamous cell carcinoma.[45] Over time, and with the rise of the -omics, the definition transitioned to “molecular alterations in […] cells that are part of histologically normal tissue.”[46] It is still under discussion whether these alterations precede cancerous lesions or are caused by them.[47] Compared to the more extensively researched concept of tumor microenvironment, these fields cover a larger area surrounding the lesion, mostly in the range of centimeters.[48–51] Field cancerization is referred to as tumor indicating normal tissue,[48,52] field defects,[53] or field effects.[47] Here, the term field effects will be used.

The examination of metabolomic field effects in prostate cancer were encouraged by studies that reported epigenomic, genomic, proteomic, and lipidomic alterations in histologically benign tissue adjacent to prostate cancer.[46,47,54] Apart from prostate cancer, metabolomic field effects were described in patients with esophageal cancer and colorectal cancer.[49–51] In prostate tissue, metabolomic cancer field effects were first mentioned in 2005 by Cheng et al. in an ^{1}H HRMAS MRS study, including 179 samples of histologically benign tissue adjacent to cancer from 82 men. In univariate analysis, two principal components (PCs) separated GS 6 and 7 ($p < 0.008$). One PC reflected changes in polyamines and citrate.[32] Later on, ^{1}H HRMAS MRS studies by Vandergrift et al. and Stenman et al. confirmed that metabolomic levels in histologically benign tissue adjacent to cancer vary with the GS of nearby cancer. Key metabolites were myo-inositol and choline.[48,55] Vandergrift et al. collected samples of histologically benign tissue adjacent to cancer from 158 prostate cancer patients: 179 samples for training and 159 samples for testing.[55] In this study, prostate cancer prognostic grade groups (PCPGG), which is a score that evolved from GS, was used for grading.[56] In univariate analysis, the region representing myo-inositol, glycerophosphocholine, phosphocholine, and valine was significantly elevated in PCPGG 1 and 2, compared to 3 and 4 (testing cohort $p < 0.0001$ and area under the receiver operating characteristic (AUROC) 0.705).[55] Stenman et al. included 40 patients and collected 41 cancer samples and 108 samples of histologically benign tissue adjacent to cancer. The metabolomic profiles of the histologically benign tissue adjacent to cancer could significantly discriminate GS 6 and 7 based on the ratios of myo-inositol/scyllo-Inositol and choline/creatine (OR 0.22, $p = 0.002$

and OR 12.8, $p < 0.001$, respectively). Interestingly, at the same time, this separation was not possible in analyses that included the cancer samples only.[48] Furthermore, Cheng et al. and Vandergrift et al. reported successful correlation of metabolic data from the histologically benign tissue adjacent to cancer with BCR, PSA, perineural invasion, and pT stages.[32,55] Stenman et al. also reported metabolomic differences in samples of histologically benign tissue adjacent to cancer collected from different distances to the cancerous lesion (myo-inositol/scyllo-Inositol ($b = 0.1$, SE $b = 0.11$, $p = 0.03$) and (glycerophosphocholine + phosphocholine)/creatine ($b = -0.46$, SE $b = 0.11$, $p < 0.001$).[48]

A possible confounding factor not considered by most of the studies mentioned above is tissue composition. Prostate tissue samples are composed of different percentages of stroma and glands. The metabolomic profiles of these components vary in linear regression, for example the levels of citrate and polyamines (glands: $r = 0.381$, $p < 0.0001$; stroma: $r = -0.303$, $p < 0.0001$).[32] The fact that the metabolomic profile that differentiates stroma vs. glands and the metabolomic profile that characterizes cancer tissue vs. histologically benign tissue have overlapping key metabolites, highlights the need to take tissue composition into account.[48] Interestingly, subgroups of cancerous tissue with the same percentage of cancerous tissue have greater metabolomic inter-sample variability than benign samples with varying percentages of glands and stroma.[48] This may explain the better performance of histologically benign samples to be separated based on GS of an adjacent lesion compared to analysis within cancer samples, that was reported by Stenman et al. reported.[48]

The studies on prostate cancer field effects leave unanswered questions. Cheng et al. and Vandergrift et al. did not measure the distance between the histologically benign samples and the lesions. Stenman et al. did not quantify the distance in total numbers.[32,48,55] No study has examined whether the correlation of metabolomic levels in histologically benign tissue adjacent to cancer with characteristics of the cancerous lesion depends on the distance from or the extent of the closest cancer. In this work, motivated by the urgent need to improve prostate cancer detection and assessment of aggressiveness, we will explore whether metabolomic profiles in histologically benign tissue can inform us on the presence and characteristics of a nearby cancer and whether these effects are distance-related. The data presented here were published in 2019 in NMR in Biomedicine.[26]

2. Methods

2.1. Patient recruitment and collection of clinical data and samples

Partners Human Research Committee, an institutional review board at Massachusetts General Hospital (MGH) in Boston, USA, approved this study. All steps were carried out according to the guidelines and regulations. All participating men gave informed, written consent to an MGH staff physician before surgery. Criteria for inclusion were a past diagnostic needle biopsy positive for prostatic acinar adenocarcinoma, no prior prostate cancer treatment, and an upcoming laparoscopic radical prostatectomy without robotic assistance. After inclusion, clinical data was obtained from Partners HealthCare EPIC database. The recorded items included age, past medical history, present illness, medication, drug use, and prostate-cancer specific data, including histopathologic results of past biopsies, pre-surgical serum PSA, and history of PSA values. To minimize variability, all prostatectomies were conducted by one of two surgeons, and one pathologist did all postsurgical sectioning. All three of them are highly competent MGH staff members, each with over ten years of experience. Starting immediately after surgical removal, the organs were kept at 4°C. Examination of specimen and sectioning was conducted mostly within 30 minutes post-removal and within one hour at most. A delay time of that magnitude was shown to have a negligible effect on metabolomic measurements.[57] Parameters were recorded following the Protocol of the College of American Pathologists, including weight and size.[58] The organs' lobes were inked in different colors, and the apex and base were sectioned off (Fig. 2). Then, the organs were cut into quarters and four transversal slices per quarter. Subsequently, one sample of 5 mm x 5 mm x 5 mm was taken per slice, making a total of 16 samples per organ. Samples were taken approximately 3 mm away from the margin where the peripheral zone is located, reflecting a trade-off of collecting tissue from where most cancers occur in the organ and preserving surgical margins for standard histopathological procedures. As shown in Fig. 2, size and orientation were captured on pictures during all steps to allow for the organs' later virtual reconstruction.

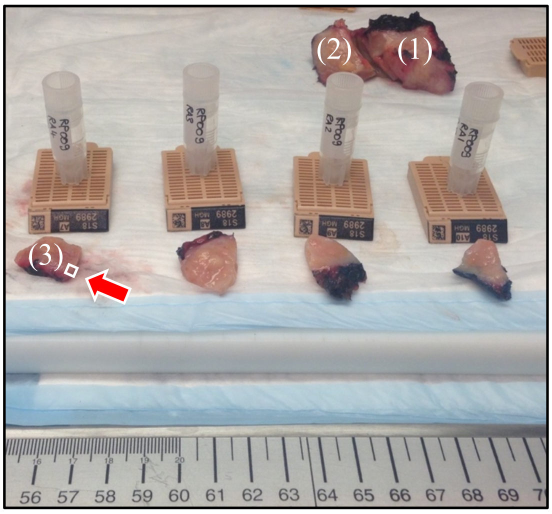

FIGURE 2. Prostate cutting. Surfaces of the right and the left lobe were inked in blue and black; the organ was cut in half (1) and quarters (2). The quarters were cut into four slices (3) and, from each slice, a sample was taken for scanning (box and arrow). Source: Personal collection.

Immediately after cutting, the 16 tissue samples were placed on dry ice and transported to the laboratory, where samples were stored at -80°C until MRS analyses were conducted. This procedure does not significantly influence metabolomic profiles.[59] The remaining parts of the prostate specimens were directly transferred to histopathological examination, as described below. Both the samples for MRS scanning and the samples directly transferred to histopathology were labeled so that their origin could be retraced back to the specific organ.

2.2. Intact tissue MRS and data processing

Tissue samples of 10 mg were cut and weighted on dry ice without thawing and then transferred into a zirconia rotor of 4 mm with Kel-F 10 µL plastic inserts. For field locking, 1 µL D_2O (99.8%) was added. An in-house developed protocol was used for ^{1}H HRMAS MRS measurements. On a vertical Bruker (Billerica, MA) AVANCE spectrometer, metabolomic spectra were recorded at 600 MHz (14.1 T) at 4°C. The spectrometer frequency was centered on the water resonance. Data were recorded with and without water suppression, using a repetition time of 5 s and a rotor-synchronized Min(A,B) procedure spinning at 600 and 700 (±1.0) Hz.[60,61] Measurements were performed blind to the clinical and pathological status of the samples. After scanning, tissue samples were fixed in 10% formalin.

A MATLAB tool, which was built in our laboratory, was used for pre-processing the raw data. After a Fourier transformation, spectra were deposed to manual correction of phase and baseline to remove frequency artifacts.[21] The intensity values between 4.5 and 0.5 ppm, a segment in which water peaks do not overlap metabolite peaks, were fitted with the curve of Lorentzian–Gaussian line shapes. Then, the spectra were manually aligned based on the creatine peak (3.026 ppm) and the left peak of alanine (1.467 ppm). Normalization was accomplished using the creatine peak's intensity from the full integral value of the water-unsuppressed file.[23] The resulting relative intensity values were reduced by summing neighboring ppm values to obtain values with two, instead of three, digits after the point. All values smaller than 1% of the median were considered noise and set to zero.

Regions of interest (ROI) were defined by summing up neighboring columns of ppm values with values that exceeded zero in > 80% of the samples. At most, three columns were combined, reflecting a trade-off between loss of information on one hand and reducing errors from possibly imperfect spectral alignment and multiple testing on the other hand.

2.3. Histopathological examination

The scanned samples and the remaining prostatectomy specimens that were not used for MRS were subject to histopathological processing and assessment. The tissue was embedded in paraffin, cut into sections of 5 µm at intervals of 100 µm throughout the entire sample, put on glass slides, and stained with hematoxylin and eosin. A genitourinary pathologist with more than 15 years of experience, blind to the spectroscopic results, assessed the slides visually. The following parameters were recorded: GS (most predominant and second most common patterns); percentages of Gleason patterns and percentages of the components of tissue (cancer, glands, and stroma) estimated to the nearest 5%; extent of cancer classified into levels less and more (a quantitative estimation taking into account the size and scatter of the lesion); further histopathologic characteristics (intraductal carcinoma, inflammation, hyperplasia, or high-grade prostatic intraepithelial neoplasia) and the presence of nerves, blood vessels, seminal vesicles or lymph vessels. From the samples used for MRS scanning, the total area of tissue on each slide was measured using a conventional scanner and the software ImageJ.[62] Volume percentage (*Vol%*) of each tissue component (cancer, glands, and stroma) was calculated for each sample. The formula below is exemplary for an imaginary sample (*s*) with three histopathological slides, denoted by the subscripts *1* to *3*, for the type of tissue (*t*). The total area (*A*) of the specimen and the percentage (*P*) of the tissue component may vary from slide to slide. Equal height (h) is assumed for all samples.

$$Vol\%_{s,t} = \frac{P_1 \times A_1 h + P_2 \times A_2 h + P_3 \times A_3 h}{A_1 h + A_2 h + A_3 h}$$

2.4. 3D organ reconstruction and grouping of samples

Based on the pictures taken during the postsurgical sectioning, each organ was virtually reconstructed in a coordinate system with units in mm. Subsequently, the distance of scanned samples to the closest cancer was measured in three dimensions. Based on these measurements, histologically benign samples (HbABC) were subgrouped using a categorical system with a cut-off point of 5 mm (HbA, ≤ 5 mm; HbB, > 5 mm, ≤ 10 mm; HbC, > 10 mm). This threshold was set because the samples were 5 mm^3 in size, and our experimental set-up did not allow measurements of distance within the samples. Cancer samples (Ca) were subdivided according to GS (≤ 3+4, ≥ 4+3) and histologically benign samples (HbA, HbB, HbC) were subdivided according to characteristics of the closest cancer. In case several cancer nodules within one prostate had the same proximity to a histologically benign sample, the one with the highest GS or the largest extent was chosen for grouping. The groups HbB and HbC were combined (HbBC) for analyses on overall-organ levels due to small and unequal sample size.

2.5. Data analysis and biological interpretation

Regions were mean-centered and auto-scaled, meaning that the intensity value was divided by each variable's standard deviation.[63] For outlier detection visual inspection of principal component analysis (PCA) score plots and a random forest analysis with a fixed cut-off of eight were conducted.[64]

Then, the spectral regions' relative intensities and PCs with an Eigenvalue (EV) > 1 were subject to univariate analyses. For binary categorical variables (see Fig. 3 for grouping: Ca vs. HbABC, Ca subgroup GS high vs. Ca subgroup GS low, HbA subgroup GS high vs. HbA subgroup GS low, HbA subgroup extent more vs. HbA subgroup extent less, HbA vs. HbBC, HbBC subgroup GS high vs. HbBC subgroup GS low, HbABC subgroup GS high vs. HbABC subgroup GS low, HbABC subgroup extent more vs. HbABC subgroup extent less, HbBC vs. HbA subgroup GS high, HbBC vs. HbA subgroup GS low, HbBC vs. HbA subgroup extent more, HbBC vs. HbA subgroup extent less), Student's t-test (for normal distributions according to Shapiro–Wilk test, with or without equal variance) or Mann–Whitney–Wilcoxon test (for non-normal distributions) were used. For ≥ ternary comparisons (HbA vs. B vs. C), analysis of variance (ANOVA, for normal distributions) or Kruskal–Wallis–Wilcoxon test (for non-normal distributions) were used. Two-sided testing was applied. The use of Bonferroni-corrected thresholds, for example, $p < 0.000794$ for 63 defined spectral regions, is indicated in the text and figures. To generate receiver operating characteristics curves (ROC), in a first step a logistic regression based on all ROIs that were significant in the previous univariate analysis was conducted and in a second step the curves were drawn based on the fitted values.

Unsupervised and supervised multivariate analysis was then applied to all above-listed comparison groups. PCA score plots were used to assess the clustering of samples visually. Loading plots of PCs of interest helped to identify the most influential metabolites. The regions that contribute to the loading are not always listed because the nature of PCs is that they represent metabolites holistically. Partial least square discriminant analysis (PLS-DA) was conducted and validated by ten-fold cross-validation to control for overfitting. Univariate and multivariate approaches have different strengths and weaknesses for metabolomics data, as discussed elsewhere.[21,65,66] Therefore, we combined the two criteria univariate significance and Variable Importance in the Projection (VIP) > 1 in PLS-DA models to select variables of interest. This is a common approach in the field.[67]

Possible confounding factors were addressed. Inter-patient differences were excluded by conducting within-organ analyses wherever sample sizes allowed it (Fig. 4B, F, G) and by including patients as random effects in mixed models. Varying tissue composition was taken into account. First, as a proof of concept, a linear mixed-effects model was applied to identify metabolomic characteristics of the tissue component stroma. Regions (*ROI*), log-transformed if skewed, and PCs with EV > 1 were regressed against the Vol% of stroma (*stroma Vol%*). The presence of cancer (*cancer*) in the sample was used as a fixed effect and the patient as a random effect

$$((ROI \text{ or } PC) \sim stroma\ Vol\% + cancer + (1|patient)).$$

Significance was tested with the likelihood-ratio test, meaning that the model without *stroma Vol%*, called null model, was compared to the model with the factor. Second, all compared groups were tested for differences in Vol% of stroma using the above-listed univariate approaches. Moreover, all comparisons conducted previously with samples stratified for stroma Vol% were re-run.

The assignment of ppm values to metabolites and metabolites to pathways was conducted based on the Human Metabolome Database (HMDB) and the Kyoto Encyclopedia of Genes and Genomes (KEGG), as well as existing literature.[68,69] We name the metabolites in Fig. 4 and, when relevant, in the discussion. In the results section, ppm values are used. Statistical analyses were performed using the R environment and the web-based platform MetaboAnalyst.[70,71]

3. Results

3.1. Patients and samples

160 samples were collected from ten organs (size: median 92 cm^3, range 33.75–141.75 cm^2; weight: median 50.5 g, range 33.8–70 g) from patients with prostatic acinar adenocarcinoma (age: median 62 years, range 53–77 years). Pathological characteristics were recorded, including percentage of organ affected by cancer (median 27.5%, range 10–90%), highest overall GS per organ (GS 3 + 3 number of organs n = 1, 3 + 4 n = 4, 4 + 3 n = 1, 4 + 4 n = 1, 4 + 5 n = 2, and 5 + 5 n = 1), and pT stages (pT2a n = 1, pT2c n = 5, pT3a n = 3 and pT3b n = 1). Perineural invasion (pN) was found in nine cases and lymph nodes were surgically removed in eight cases (pN1 n = 2, pN0 n = 6). In no case metastases were found during the 12 months of follow-up after organ collection. Sample information is presented in Fig. 3. Two samples were excluded prior to raw data processing due to irregularities during MRS data acquisition. Two further samples were excluded after being identified as outliers, as described in the methods section. Data processing led to 63 ROIs.

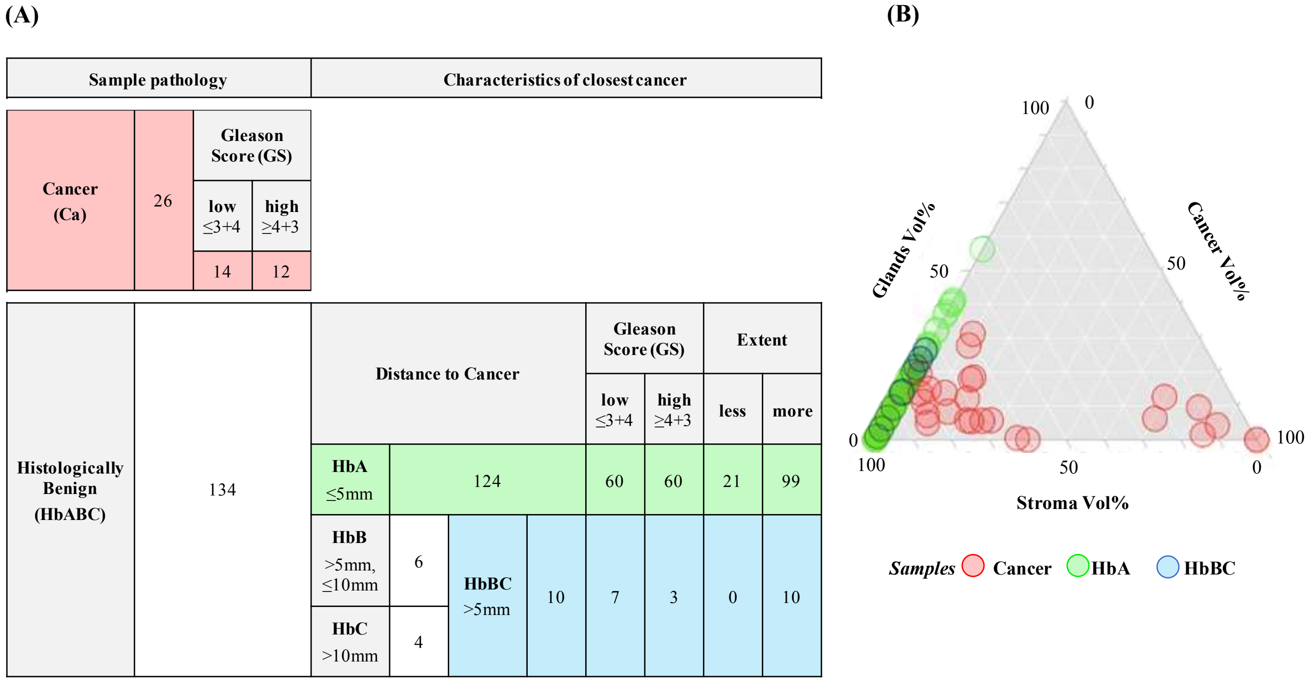

<table>
<tr><th colspan="2">Sample pathology</th><th colspan="8">Characteristics of closest cancer</th></tr>
<tr><td rowspan="3">Cancer
(Ca)</td><td rowspan="3">26</td><td colspan="2">Gleason Score (GS)</td><td colspan="6"></td></tr>
<tr><td>low
≤3+4</td><td>high
≥4+3</td><td colspan="6"></td></tr>
<tr><td>14</td><td>12</td><td colspan="6"></td></tr>
<tr><td rowspan="5">Histologically Benign
(HbABC)</td><td rowspan="5">134</td><td colspan="4" rowspan="2">Distance to Cancer</td><td colspan="2">Gleason Score (GS)</td><td colspan="2">Extent</td></tr>
<tr><td>low
≤3+4</td><td>high
≥4+3</td><td>less</td><td>more</td></tr>
<tr><td>HbA
≤5mm</td><td colspan="3">124</td><td>60</td><td>60</td><td>21</td><td>99</td></tr>
<tr><td>HbB
>5mm,
≤10mm</td><td>6</td><td rowspan="2">HbBC
>5mm</td><td rowspan="2">10</td><td rowspan="2">7</td><td rowspan="2">3</td><td rowspan="2">0</td><td rowspan="2">10</td></tr>
<tr><td>HbC
>10mm</td><td>4</td></tr>
</table>

FIGURE 3. Sample characteristics and grouping. (A) Cancer samples (red) were grouped based on GS. Histological benign samples (green and blue) were grouped based on distance to and characteristics of the closest cancer. Due to group size, HbB and HbC were merged for overall-organ analyses. **(B)** Distribution of volume percentage (Vol%) of the tissue components cancer, stroma and glands in cancer samples (red), HbA (green), and HbBC (blue) is presented in a scatterplot. In the cancer samples, the median of Vol% cancer is 19.67 (range 2–100), of glands 7.83 (0–31.25) and of stroma 66.37 (0–83.75). In the histological benign samples, the median of Vol% glands is 9.5 (range 0–56.27) and of stroma 90.50 (43.75–100). (A) Adapted with permission from REF[26], CC BY 4.0 (https://creativecommons.org/licenses/by/4.0/). (B) Source: Personal collection.

3.2. Metabolomics differ in cancer and benign tissue and in cancer tissue of different GS

Ca and HbABC samples were visually separable in a PCA score plot. A PLS-DA model was built (R2Y = 0.33 and Q2Y = 0.18). In Bonferroni-corrected univariate analysis, two ROIs (4.34–4.32 and 3.22–3.20) were significantly different, both had a VIP > 1 and increased levels in Ca (Fig. 4A). From 12 PCs with an EV > 1, three were significantly different (PC3 $p < 0.05$, PC5 $p < 0.001$, PC6 $p < 0.0001$). Within-organ analysis confirmed that the findings were not caused by between-patient differences (PLS-DA R2Y = 0.99 and Q2Ycum = 0.45) (Fig. 4B).

Ca samples of low GS ($\leq 3 + 4$) were visually separable from Ca samples of high GS ($\geq 4+ 3$) in PCA score plots. A PLS-DA model (R2Y = 0.84 and Q2Ycum = 0.48) and Bonferroni-corrected univariate analysis revealed two significantly different regions (3.24–3.23 and 2.31–2.30), both with a VIP > 1 (Fig. 4C). The intensities of both regions increased with increasing GS. Of ten PCs with an EV > 1, two were significantly different (PC2 $p < 0.01$, PC5 $p < 0.05$).

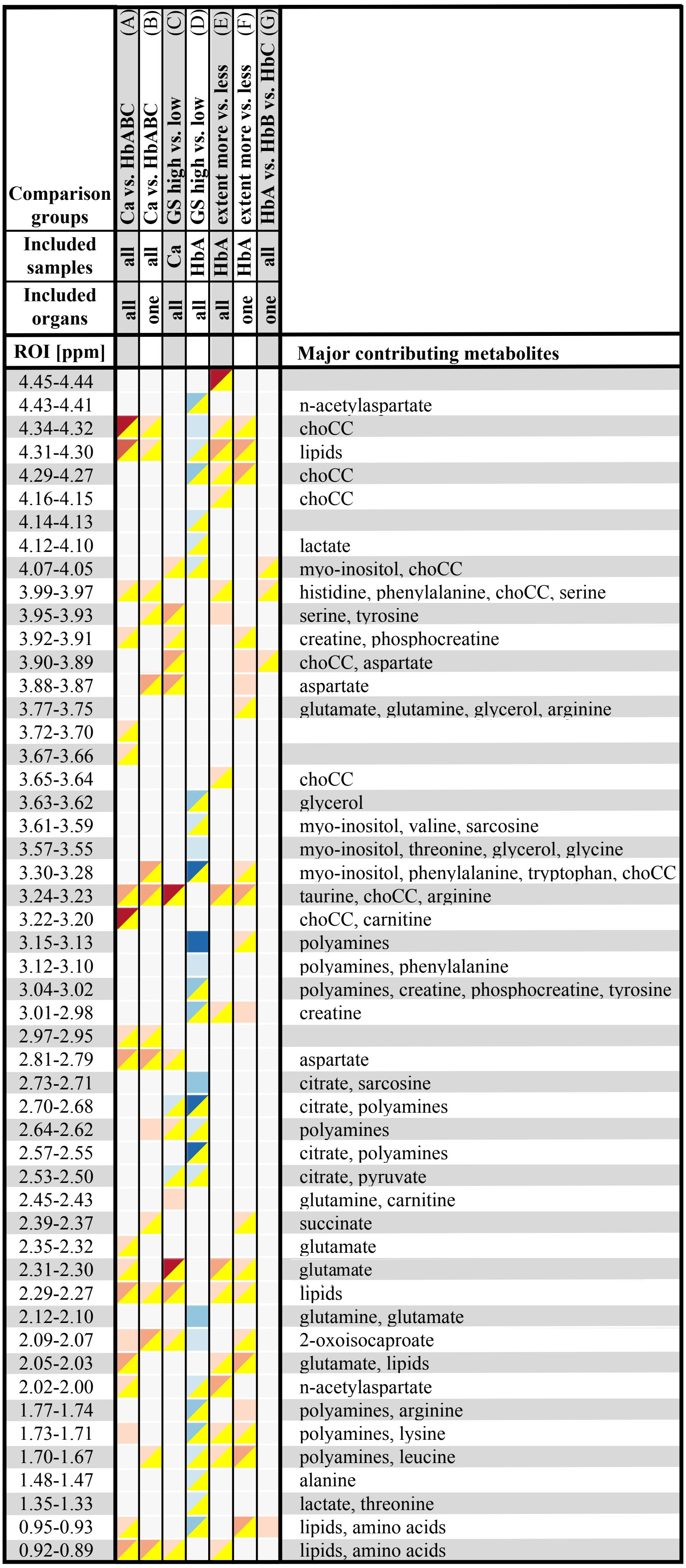

Comparison groups	Included samples	Included organs
(A) Ca vs. HbABC	all	all
(B) Ca vs. HbABC	all	one
(C) GS high vs. low	Ca	all
(D) GS high vs. low	HbA	all
(E) extent more vs. less	HbA	all
(F) extent more vs. less	HbA	one
(G) HbA vs. HbB vs. HbC	all	one

ROI [ppm]	Major contributing metabolites
4.45-4.44	
4.43-4.41	n-acetylaspartate
4.34-4.32	choCC
4.31-4.30	lipids
4.29-4.27	choCC
4.16-4.15	choCC
4.14-4.13	
4.12-4.10	lactate
4.07-4.05	myo-inositol, choCC
3.99-3.97	histidine, phenylalanine, choCC, serine
3.95-3.93	serine, tyrosine
3.92-3.91	creatine, phosphocreatine
3.90-3.89	choCC, aspartate
3.88-3.87	aspartate
3.77-3.75	glutamate, glutamine, glycerol, arginine
3.72-3.70	
3.67-3.66	
3.65-3.64	choCC
3.63-3.62	glycerol
3.61-3.59	myo-inositol, valine, sarcosine
3.57-3.55	myo-inositol, threonine, glycerol, glycine
3.30-3.28	myo-inositol, phenylalanine, tryptophan, choCC
3.24-3.23	taurine, choCC, arginine
3.22-3.20	choCC, carnitine
3.15-3.13	polyamines
3.12-3.10	polyamines, phenylalanine
3.04-3.02	polyamines, creatine, phosphocreatine, tyrosine
3.01-2.98	creatine
2.97-2.95	
2.81-2.79	aspartate
2.73-2.71	citrate, sarcosine
2.70-2.68	citrate, polyamines
2.64-2.62	polyamines
2.57-2.55	citrate, polyamines
2.53-2.50	citrate, pyruvate
2.45-2.43	glutamine, carnitine
2.39-2.37	succinate
2.35-2.32	glutamate
2.31-2.30	glutamate
2.29-2.27	lipids
2.12-2.10	glutamine, glutamate
2.09-2.07	2-oxoisocaproate
2.05-2.03	glutamate, lipids
2.02-2.00	n-acetylaspartate
1.77-1.74	polyamines, arginine
1.73-1.71	polyamines, lysine
1.70-1.67	polyamines, leucine
1.48-1.47	alanine
1.35-1.33	lactate, threonine
0.95-0.93	lipids, amino acids
0.92-0.89	lipids, amino acids

🟥 Bonfer.
🟥 $p < 0.001$
🟥 $p < 0.01$
🟥 $p < 0.05$

Higher in first-mentioned group
e.g. in column (A), the level of 4.34-4.32 is higher in subgroup Ca

🟦 Bonfer.
🟦 $p < 0.001$
🟦 $p < 0.01$
🟦 $p < 0.05$

Lower in first-mentioned group
e.g. in column (D), the level of 4.43-4.41 is lower in subgroup GS high

◢ PLS-DA VIP>1

FIGURE 4. Univariate and multivariate results. For the analysis presented in column (A) to (G), the top rows indicate included organs, included samples and comparison groups. Results of univariate (red, blue) and multivariate PLS-DA (yellow) analyses are color-coded. For overall-organ analyses, sample sizes can be found in Fig. 3A. Within-organ analyses, conducted when samples sizes allowed it, are presented in columns (B), (F) and (G): **(B)** Ca n=9, HbABC n=7, all histologically benign samples were adjacent to a cancer lesion of extent more; **(F)** HbA subgroup extent more n = 9, HbA subgroup extent less n=5, all histologically benign samples were adjacent to cancer of GS low; **(G)** HbA n=8, HbB n=3, HbC n=4. Levels of significance: 4.07–4.05 between HbA, HbB, and HbC, 0.95–0.93 between HbA and HbB; 3.99–3.97 and 3.90–3.89 between HbA and HbC only. Assignment of ROIs to metabolites was done wherever possible. *choCC, choline containing compounds and choline; amino acids, mainly leucine, valine, and isoleucine.* Adapted with permission from REF[26], CC BY 4.0 (https://creativecommons.org/licenses/by/4.0/).

3.3. Metabolomics in histologically benign tissue close to cancer (≤5 mm) vary with GS and extent of the closest lesion

Within the group of histopathological benign samples, the two comparison groups extent of cancer (levels less and more) and GS (levels high and low) were not correlated. Visual inspection of the HbA samples' PCA score plots showed trends of separation of HbA subgroup GS high vs. HbA subgroup GS low. The same applies for HbA subgroup extent more vs. HbA subgroup extent less. Multivariate models were built (GS high vs. low R2Y = 0.07 and Q2Y = 0.02; extent more vs. less R2Y = 0.06 and Q2Y = 0.02). In a Bonferroni-corrected univariate analysis the regions 3.30–3.28, 2.70–2.68, and 2.57–2.55 were negatively correlated with GS (Fig. 4D), while the region 4.45–4.44 was positively correlated with the extent of cancer (Fig. 4E). All of them had a VIP > 1. From 11 PCs with an EV > 1 within the group of HbA, PC1 ($p < 0.05$) was significantly different in both extent more vs. less and GS high vs. GS low, while PC6 ($p < 0.01$) was only significantly different in extent more vs. less. A within-organ analysis confirmed metabolomic separability of HbA subgroup extent more vs. less (Fig. 4F). The groups were visually separable in a PCA score plot. 16 ROIs differed in univariate analysis. All of them had a VIP > 1 (PLS-DA R2Y = 0.582 and Q2Y = 0.153), but lost significance after Bonferroni correction. Nine ROIs were overlapping in within-organ and overall-organ analyses. Of seven PCs with an EV > 1, PC1 was significantly different ($p < 0.05$). Due to sample availability, no within-organ analysis could be conducted for HbA subgroup GS high vs. low.

3.4. Metabolomics in histologically benign tissue vary with distance from closest cancer

Due to the small sample sizes, samples at distances > 5 mm and ≤ 10 mm (HbB) and > 10 mm (HbC) were grouped for the overall-organ analysis (HbBC). The two groups HbA vs. HbBC showed trends of separation in a PCA score plot. Univariate analysis based on all organs showed that the regions 0.97–0.96 ($p < 0.01$); 2.02–2.00, 4.29–4.27, 4.31–4.30, 4.16– 4.15 and 0.92–0.89 ($p < 0.05$) all decreased in intensity with increasing distance from the cancer (HbA to HbBC). The unequal group size of HbBC (n = 10) vs. HbA (n = 124) did not allow us to build a multivariate model. In order to offer a multivariate perspective nonetheless, the loading plot of a PC that was significantly different in univariate analysis after Bonferroni correction is given in Fig. 5. Metabolites that had both high loading in PCA and significance in univariate analysis are highlighted. On the organ level, HbA (n = 8), HbB (n = 3) and HbC (n = 4) were compared. For representative spectra from this organ, see Fig. 1. The groups were visually separable in PCA score plots, and PC2 was significantly different ($p < 0.05$). In univariate analysis, three ROIs differed (4.07–4.05, 3.99–3.97, and 3.90–3.89 ppm), all of them had a VIP > 1 (R2Y = 0.634 and Q2Y = 0.18) but lost significance after Bonferroni correction (Fig. 4G). All three ROIs showed decreasing concentrations with increasing distance from the cancer. The comparability of within-organ and overall-organ analysis is limited as for latter HbB and HbC were merged. Still, it is noteworthy that although the differentiating metabolites of within organ (see Fig. 4G) and overall-organ (see Fig. 5) vary partly, the differentiating regions that do not overlap are neighboring.

3.5. Metabolomic variation in histologically benign tissue with GS and extent of the closest cancer is less prominent at a greater distance from the cancer (> 5 mm)

Contrary to HbA, the metabolomic profiles of HbBC samples did not vary with the GS of the closest cancer. No multivariate model could be built. Only two regions were significantly different in univariate analyses between HbBC close to GS high vs low, but barely exceeded the level of significance (2.81–2.79, 2.17–2.16, $p < 0.05$; increased in the subgroup GS high) and lost significance after Bonferroni correction. The weaker performance of HbABC to distinguish GS high vs GS low of a nearby cancer compared to the performance of HbA is underlined by ROCs: Within HbA subgroup GS high vs. subgroup GS low AUROC = 0.830 (95% CI, 0.76–0.91) and within HbABC subgroup GS high vs. subgroup GS low AUROC = 0.765 (95% CI, 0.69–0.85). Similarly, a PLS-DA model based on HbABC samples was weaker than HbA samples only (HbABC, R2 = 0.0631and Q2 = 0.0021 vs. HbA, R2Y = 0.07 and Q2Y = 0.02).

In line with these findings, the performance of HbABC to distinguish the extent of a nearby cancer was weaker than in analyses based on HbA only: 1.73–1.71 and 0.92–0.89 lost significance in univariate analysis, and one newly significant region appeared at a very low level of significance (3.67–3.66 ppm, $p = 0.044$; concentration higher in subgroup extent more). No PLS-DA model could be built. Due to sample size, no analysis could be conducted in HbBC only. The AUROC was smaller within HbABC (AUROC = 0.870 [95% CI, 0.80–0.94]) compared to HbA (AUROC = 0.918 [95% CI, 0.86–0.98]). After finding that HbBC does not, or does but only to a small extent, vary with GS and extent, but that HbA does, we conducted analyses of HbBC vs. following subgroups of HbA: HbA subgroup GS high, HbA subgroup GS low, HbA subgroup extent more, and HbA subgroup extent less. PC7 was significantly different between HbBC compared to each of the subgroups as well as in HbBC vs. HbA. The major contributing regions of PC7 are labeled in Fig. 5.

Interestingly, in univariate analysis no difference could be found in HbA subgroup extent less vs. HbBC, whereas HbA subgroup extent more differed significantly from HbBC (4.31–4.30, 4.29–4.27, 4.16–4.15, 2.02–2.00, 0.97–0.96 and 0.92–0.89, $p < 0.05$; all increased in HbA). There were significant differences in univariate analysis between HbBC vs. HbA subgroup GS low (4.29–4.27 $p < 0.01$; 0.97–0.96, 4.43–4.41, 4.31–4.30, 3.01–2.98 and 2.02–2.00 $p < 0.05$; all increased in HbA) and between HbBC vs. HbA subgroup GS high (0.97–0.96 $p < 0.05$; decreased in HbA).

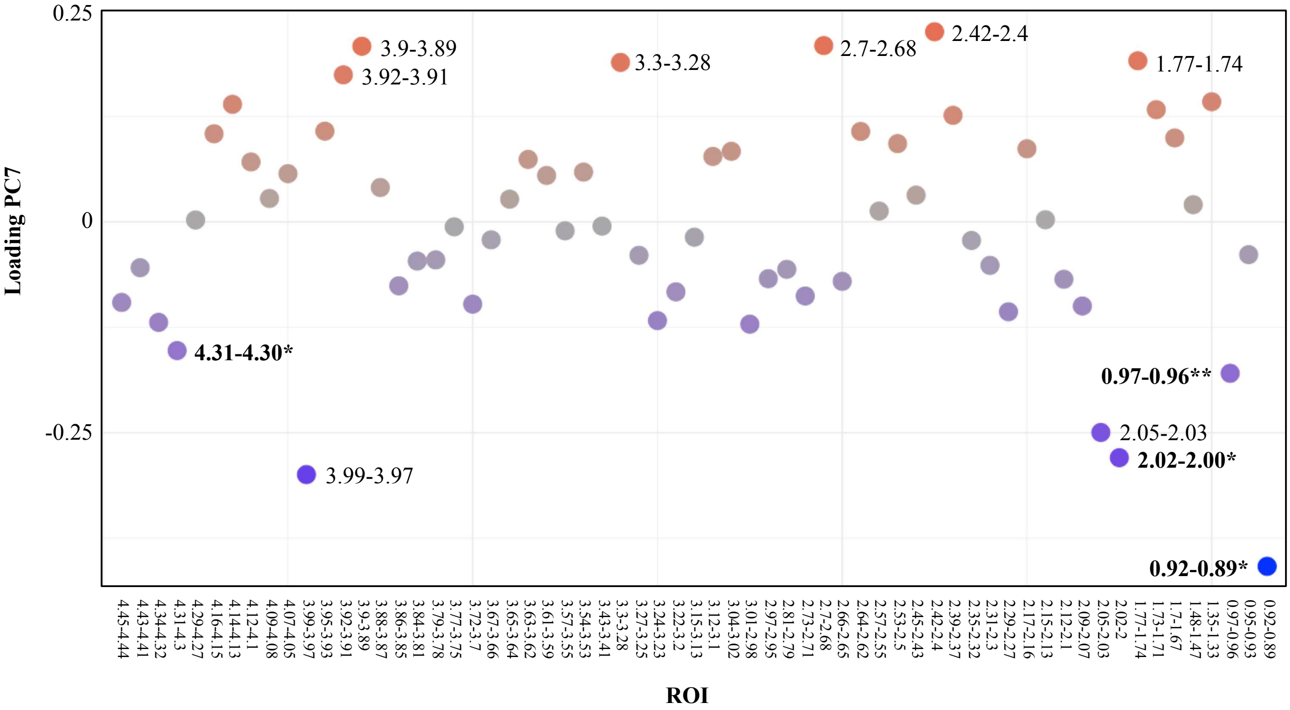

FIGURE 5. Loading plot of PC7 of PCA based on all benign samples (HbABC). In univariate analysis, PC7 was significantly different between HbA and HbBC ($p < 0.05$ after Bonferroni correction) and between HbBC vs. each of the subgroups of HbA (GS high, GS low, extent more, extent less). The most influential regions are labeled and the regions among them that also differed significantly in univariate analysis of HbA vs. HbBC are printed bold. *Red, positive loading value; blue, negative loading value; * $p < 0.05$, ** $p < 0.01$.* Source: Personal collection.

3.6. Influence of tissue composition

A mixed model revealed metabolic differences between tissue components. The following ROIs differed significantly based on stroma Vol% after Bonferroni-correction: 3.15-3.13 ($\chi^2(1)=26.19$), 3.12-3.10 ($\chi^2(1)=29.72$), 2.73-2.71 ($\chi^2(1)=24.71$), 2.57-2.55 ($\chi^2(1)=28.62$), 2.12-2.10 ($\chi^2(1)=21.14$), 2.09-2.07 ($\chi^2(1)=20.00$), 1.77-1.74 ($\chi^2(1)=20.15$) and 1.48-1.47 ($\chi^2(1)= 16.38$), ($p < 0.0001$); and 4.34-4.32 ($\chi^2(1)=13.47$), 3.61-3.59 ($\chi^2(1)=14.39$), 3.22-3.20 ($\chi^2(1)=14.98$), 2.70-2.68 ($\chi^2(1)=12.17$), 2.53-2.50 ($\chi^2(1)=10.96$), 2.31-2.30 ($\chi^2(1)=14.32$), 2.05-2.03 ($\chi^2(1)=11.62$), 1.73-1.71 ($\chi^2(1)=11.11$), 1.70-1.67 ($\chi^2(1)=13.95$), 0.97-0.96 ($\chi^2(1)= 11.40$), ($p < 0.001$). All ROI decrease in intensity with increasing stroma Vol%. One PC was significantly affected by stroma Vol% (PC1 ($\chi_2(1)=18.46$), $p < 0.0001$). Its major contributing metabolites in the loading plot also appear among the above listed significant metabolites, namely 2.09–2.07, 2.12–2.1, and 3.61–3.59 (loading decreasing).

Then, all compared groups reported in the results sections were univariately tested for differences in stroma Vol%. We found no significant differences, exemplarily shown for one ROI in Fig. 6A.

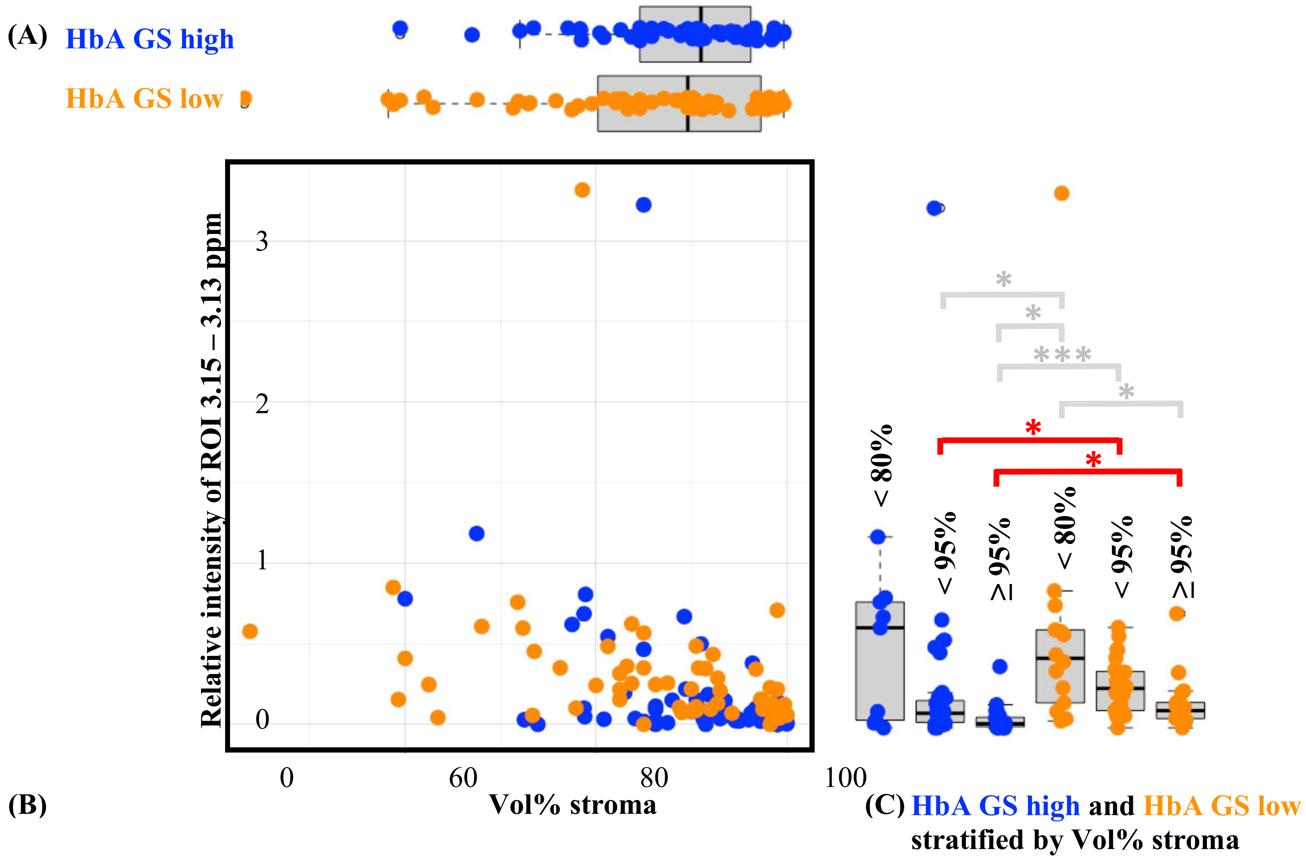

FIGURE 6. Influence of varying Vol% stroma on HbA. (B) HbA samples, colorcoded for subgroups based on the GS of an adjacent lesion (*low,* $\leq 3+4$*, orange; high,* $\geq 4+3$*, blue*) are presented in a scatterplot. The subgroups **(A)** do not differ in Vol% stroma, **(C)** but do differ significantly in relative intensity in ROI 3.15–3.13 in analysis stratified for Vol% stroma, but only in Vol% stroma > 80%. *Red and grey brackets, levels of significance in univariate analysis;* * $p < 0.05$, ** $p < 0.01$, *** $p < 0.0001$. Source: Personal collection.

For all reported comparisons, all regions previously identified as significant were tested again in groups stratified for stroma Vol%. This is presented exemplarily in Fig. 6C for ROI 3.15–3.13 and the comparison HbA subgroup GS high vs. HbA subgroup GS low. For the comparisons within histologically bening samples (HbA, HbB and HbC), all ROIs remained significant in stroma Vol% > 80%; in stroma Vol% < 80% significance was lost in most of the ROIs.

4. Discussion

4.1. Biological interpretation of the findings

This study evaluated the diagnostic and prognostic utility of prostate tissue metabolite profiles measured in histologically benign tissue with high-field (14.1 T) ^{1}H HRMAS MRS. We reported (1) the proof of concept that cancer vs. histologically benign tissue as well as cancer tissue of low vs. high GS are metabolomically different; (2) that metabolomics in histologically benign samples adjacent to cancer vary with characteristics of cancer (extent and GS), but—and this has not been previously published—only if the distance from the cancer is small ($\leq$ 5 mm); and (3) that histologically benign samples are significantly different at different distances from the cancer ($\leq$ 5 mm vs. $>$ 5 mm and $\leq$ 10 mm vs. $>$ 10 mm). Interestingly, the differences between histologically benign tissue close to a cancerous lesion ($\leq$ 5 mm) and tissue at a greater distance ($>$ 5 mm) were more prominent in tissue adjacent to cancer of a larger extent. Possibly, a certain amount of prostate cancer mass is needed to produce these effects. For the first time, metabolomic prostate cancer field effects were reported in within-organ analyses in the work presented here. The effects were stable in analyses matched for tissue composition of stroma and glands, but, of note, the effects in histologically benign tissue were more prominent in samples with higher percentages of stroma.

Although we seek to report metabolomic profiles rather than individual metabolites, key discriminatory metabolites are summarized here: For cancer vs. histologically benign, choline, choline containing compounds, aspartate and lipids (Fig. 7B, underlined) and for cancer tissue of low vs. high GS, aspartate, taurine and glutamate. In histologically benign tissue, myo-inositol, polyamines and citrate correlated with the GS, and taurine and polyamines correlated with extent of a nearby cancer. Lipids, myo-inositol and choline and choline containing compounds varied with the distance between the histologically benign sample and the cancerous lesion.

Physiologically, the metabolism of prostatic glandular epithelium differs from other mammalian cells. It is characterized by enhanced aerobic glycolysis, diminished oxidative phosphorylation, and a truncated tricarboxylic acid (TCA) cycle (Fig. 7A). Zinc impairs m-aconitase, which enables citrate to be used as an end-product for secretion into the prostatic fluid or, to a lesser extent, an intermediate for lipid synthesis. The TCA cycle is supplied with precursors, including oxaloacetate from aspartate and alpha-ketoglutarate from glutamate. In malignant prostate cells, zinc is no longer accumulated. The activity of the TCA cycle and oxidative phosphorylation increase.[72,73] Hence, the levels of citrate and the end-products of anaerobic glycolysis, lactate and alanine, decrease.[74] Glycolysis is downregulated, and, instead of glucose, fatty acids serve as dominant substrates (Fig. 7B).[75] Of note, in highly advanced cancer, metabolic alterations may occur such as the Warburg effect and a decrease of the activity of the mitochondrial creatine kinase.[72,76]

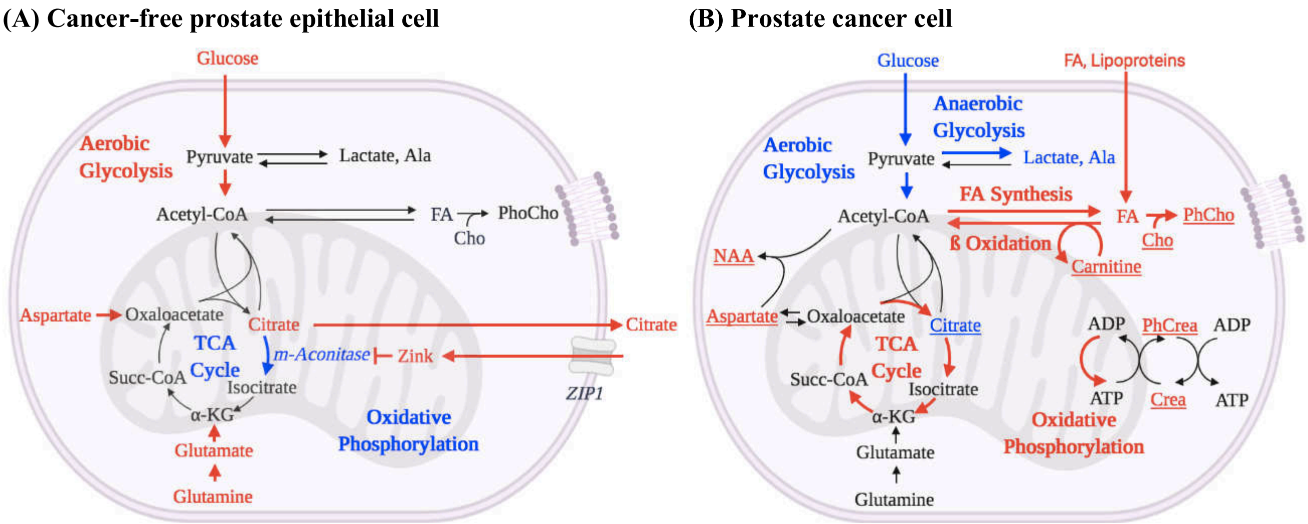

(A) Cancer-free prostate epithelial cell

(B) Prostate cancer cell

FIGURE 7. Selected metabolic processes in healthy prostate epithelial cells and in low-grade prostate cancer cells. (A) Cancer-free prostate epithelial cells are metabolomically unique with high aerobic glycolysis and low oxidative phosphorylation. Zinc inhibits m-aconitase and impairs the TCA Cycle. *Compared to other mammalian cells: red, incrased; blue, decreased.* **(B)** In prostate cancer cells citrate is oxidized in the TCA Cycle, glucose uptake is decreased, and fatty acids are the main substrates for energy production. De novo lipogenesis and oxidative phosphorylation are enhanced. *Compared to (A): red, incrased; blue, decreased (according to the literature); underlined, univariate differences between Ca and HbABC in the data presented in this study (Fig. 4A). α-KG, α-ketoglutarate; Ala, alanine; Cho, choline; Crea, Creatine; FA, fatty acids; NAA, n-acetylaspartate; PhCrea, phosphocreatine; PhoCho, phosphatidylcholine; Succ-CoA, Succinyl-CoA; TCA, tricarboxylic acid; ZIP1, zinc transporter 1.* Source: Personal collection.

In line with the described alterations of the TCA cycle in cancer cells, decreased levels of citrate in cancerous tissue vs. histologically benign[25,33,41,42] (Fig. 7B), and in cancerous tissue of higher vs. lower GS were reported here and in other studies.[25,33,41,42,77] Here and in previously published studies, levels of citrate in histologically benign tissue correlate negatively with the GS of an adjacent cancer.[32,48] Alterations of the anaplereutic metabolites for the TCA cycle were reported here and in other publications: Aspartate was increased in cancer vs. benign (Fig. 7B)[78] and in cancer tissue of high vs. low GS. Glutamate and glutamine correlated with the extent and GS of a nearby lesion in histologically benign tissue adjacent to cancer.

Previously described alterations of lipid metabolism in prostate cancer include upregulated de novo lipid biosynthesis possibly for membranogenesis, a prerequisite for proliferation, and for fatty acid ß-oxidation for ATP-production.[79] Here and in previous studies, lipids were increased in cancer compared to histologically benign tissue[38,39,77,80] (Fig. 7) and in cancerous tissue of high GS vs. low GS.[37,78] In histologically benign tissue adjacent to cancer, lipids correlated positively with the extent of cancer and negatively with the GS of and distance to cancer. Correlations between levels lipids in histologically benign tissue and grades of a nearby prostate cancer were reported in previous publications.[81]

The carnitine cycle regulates fatty acid mitochondrial import and export and was shown to be upregulated in prostate cancer.[81,82] In line with other publications, we found higher levels of carnitine in cancer vs. histologically benign tissue (Fig. 7B)[35,37,80] and in cancer of high vs. low GS.[38]

Phospholipid metabolism with its key enzyme choline kinase, which synthesizes constituents of cell membranes, is known to be upregulated in prostate cancer.[79] Choline has even been successfully used as an alternative tracer for positron emission tomography (PET) imaging[81] and was suggested to serve as biomarker for in vivo prostate spectroscopy[84]. In our dataset and other studies, choline and choline-containing metabolites were increased in prostate cancer tissue compared to healthy controls (Fig. 7B);[25,32,33,36,39,41,42,77,80,85] they positively correlated with GS both in cancer [25,33,42,77] and histologically benign tissue[48,55] and negatively correlated with distance to cancer in histologically benign tissue[48]. Paracrine introduction of changes in the choline phospholipid metabolism in adjacent histologically benign cells could be an explanation for the alterations that we found in histologically benign tissue adjacent to cancer.[84] It has been suggested that choline is more suitable as a biomarker than, for example, citrate because it varies much less between stromal and glandular tissues.[25,48,85,86]

Increased levels of n-acetylaspartate (NAA) in prostate cancer compared to histologically benign tissue, which we and other studies reported (Fig. 7B)[80], could reflect a general increase of metabolic rates in rapidly dividing cells, or specific changes associated with the oncogenic process.[39,87] In neural tissue, NAA provides acetate for the synthesis of fatty acids, and in lung cancer, it may regulate the utilization of nutritients including glutamine.[87] In our dataset, NAA was also major contributing metabolite to the PC that separated histologically benign samples at different distances to cancer. Furthermore, levels of NAA in histologically benign tissue correlated positively with GS and correlated negatively with the extent of the closest cancer.

Creatine is important in energy metabolism, as phosphocreatine supplies phosphate to ADP to gain ATP.[88] In prostate cancer, mitochondrial creatine kinase was shown to have increased activity compared to histologically benign.[76] Accordingly and in line with other publications, we reported elevated levels of creatine in cancer compared to histologically benign samples (Fig. 7B).[42,80] Furthermore, levels in cancer samples correlated positively with GS[42] and levels in histologically benign tissue varied with increasing distance from the cancer.[47]

The polyamines putrescine, spermidine, and spermine are involved in processes of cell growth and survival.[89] Spermine, which is secreted into the prostatic fluid, has a higher concentration in the prostate than in any other organ.[80] Spermine has cytostatic and cytotoxic effects and was suggested to be an endogenous inhibitor of prostate cancer growth. Concentration in tissue were previously reported to correlate with the volume of healthy, cancer-free prostatic epithelial cells.[80,90] In our dataset, levels of polyamines in histologically benign tissue increased with the GS of an adjacent cancer, a finding supported by previous publications.[32,55]

Myo-inositol is involved in osmo- and volume regulation and cell signaling, for example, the oncogenic PI3K pathway.[48] It may be an endogenous tumor suppressor.[55] In our dataset, levels of myo-inositol in histologically benign tissue decreased with the GS of an adjacent cancer and increased with distance to cancer, findings supported by previous publications.[48,55,91]

Taurine, a non-essential amino acid effecting oxidative processes, immune surveilance and apoptosis, was suggested to be crucial in prostate cancer regulation.[80,92] Here and in previous publications, levels of taurine were significantly different in cancer compared to histologically benign tissue.[80,85,93] As the ROI that represents taurine also contains signals from choline and choline containing compounds in the data presented here, the direction of fold change cannot be interpreted clearly. Furthermore, we reported altered levels of taurine in cancerous tissue of high vs. low GS and in histologically benign tissue close to cancer of extent more vs. extent less.

In our dataset, key metabolites that differed between the tissue compartments stroma and glands, were polyamines and citrate, all decreasing with the Vol% of stroma. Previous studies are in line with these findings.[25,32,77,85,86] A methodological standardization for the handling of varying percentages of stroma and glands in HRMAS MRS studies is yet to be established. Some studies do not take this possible confounding factor into account at all, others stratified the samples for tissue components prior to the analysis[94] or, and this approach was chosen in the work presented here, did a second round of analysis to control if the findings remain significant in groups stratified for tissue composition.[55] Other authors suggested to take only those metabolites into consideration as biomarkers that do not vary at all between tissue components.[48] Ideally, metabolomic variation due to different tissue components could be excluded prior to statistical analysis. Of great help would be a description of each component's pure spectra. This could be achieved by matrix-assisted MS combined with microscopic assessment.[80,95,96] These pure spectra could serve as a baseline, similar to the idea behind the human genome project. For a given tissue sample, one could calculate the cancer-free profile (e.g., 30% stroma and 70% glands). The aberrations would largely reflect the variations of interest, for example, cancer vs. benign.

Furthermore, open to further research remains the question of the cancer fields' origin. On the one hand, other -omic levels offer evidence that field effects constitute precancerous lesions.[47] On the other hand, alterations might be the response of neighboring tissue to the cancerous lesion. It has also been suggested that low-weight molecules could migrate from the cancer to its surroundings.[97] Processes in the surrounding stroma were discussed under the name "reactive stroma," possibly induced via TGFß[98,99] and promoting, in turn, angiogenesis and tumorigenesis. The reactive stroma concept is in line with the tissue organization field theory (TOFT). It states that cancer is a tissue-based, instead of cell-based, disease, in contrast to the well-known somatic mutation theory.[100] Most probably, the phenomena that have so far been subsumed under the term "field effects" are partly precancerous conditions and partly induced by a nearby cancerous lesion. Deeper understanding could be gained, for example, by a simultaneous collection of data on several -omic levels. Some studies have shown successful combinations of metabolomics and transcriptomic,[36,99,101] genomic,[102,103] or immunohistochemical data.[34] Another approach would be a thorough examination of cancer-free organs, possibly from organ donors. Metabolomic fields that precede prostate cancer could be detectable, although the time of ischemia could influence the data. Moreover, longitudinal study designs could help. For example, in a nested case-control study, men with the same likelihood for prostate cancer detection would undergo several biopsies at different points along a timeline. The men that are subsequently diagnosed with prostate cancer would make up the group "cases," while the ones that remain cancer-free would be the "healthy controls."

4.2. Limitations and weaknesses

A limitation of the work presented here is that some groups were relatively small and of unequal sizes, such as samples at a larger distance than 5 mm from prostate cancer. This is due to the multifocality of prostate cancer. Consequently, it was not possible to divide the dataset into a training and a testing cohort. Instead we evaluated the models by ten-fold cross-validation. Moreover, PLSDA, being vulnerable to unequal group sizes, could not be conducted for all comparison groups.[59] To gain a multivariate perspective nevertheless, PCs were subject to univariate analysis.

In addition, 5-mm steps for grouping the samples for distance to cancer are relatively large. Experimental designs with smaller tissue samples could help. A software-based reconstruction of the organs could improve accuracy further.[106]

Furthermore, we did not include tissue from cancer-free organs as a control group. These could be obtained from cystoprostatectomy in bladder cancer surgery, however, samples could be impaired by the patients' age, the bladder cancer or treatment, or from organ donors, but the time of ischemia could be a limiting factor. Biopsies from healthy men are not feasible due to invasiveness.[47]

Finally, there are widely acknowledged weaknesses in the field of metabolomics in general. There is a lack of methodological standardization. There is reason to be optimistic, however, as initiatives like Coordination of Standards in Metabolomics (COSMOS) are developing guidelines; open-access tools for reproducible data processing and analysis, such as MetaboAnalyst and a multitude of R packages, are becoming more widely used; and databases for reliable metabolite and pathway assignments are constantly growing, including KEGG and HMDB.[68–71,107] Statistical approaches to remove metabolomic variation due to biological factors including age, diet, medication, physical activity and genetic background are being developed and discussed in the literature.[108] Due to the structure of the dataset presented here with relatively few individuals and many samples per individual, we rather focused on within-organ analyses.

4.3. Scientific implications and clinical applications

The presence of metabolomic field effects challenges the use of histologically benign prostate tissue from cancerous organs as mere healthy controls. This procedure, besides the lack of methodological standardization in metabolomic studies in general, may contribute to the considerable variation among published metabolomic tissue biomarkers. This is underlined by our finding that the metabolomic profile that distinguishes histologically benign tissue in proximity vs. at greater distances to cancer and the profile that varies between histologically benign tissue and cancerous tissue have overlapping key metabolites, for example, choline and choline containing compounds (3.34–4.32 ppm and 3.22–3.2ppm). We call for researchers to take field effects into account in study design and data analysis.

The findings presented here encourage validation studies. In a clinical setting, metabolomic field effects could enlarge the target area for biopsies, reducing the number of false-negative and under-graded biopsies. Increased diagnostic accuracy of biopsies could reduce cases of undertreatment. At the same time, this approach could also help identify low-risk cancer and make active surveillance a more attractive alternative to potentially harmful procedures, thereby reducing overtreatment.[46] Once established, an approach like this could exclude men from potentially unnecessary re-biopsies and may help to reduce the number of needed biopsy cores, thereby lowering patients' biopsy-associated risks. As the acquisition of metabolomics data is near real-time metabolomic profiles could be measured during interventions. This approach could help to decide immediately during biopsy whether to resample or stop sampling. An NMR-based approach's translatable capacity is significant, as due to its non-destructive nature it can be added to the current clinical workflow of histopathological assessment without impairing it. It also requires minimal sample preparation, has high throughput, and is cost-effective, automated, and reproducible. In contrast to histopathological assessment, where GS grading shows inter-observer variations, the data is objective.[81] At present, smaller machines are being developed that are less expensive and suitable for a clinical setting.[109] This approach is in line with the precision medicine initiative that seeks individualized clinical decision-making to find the best strategy for each individual patient.

The ultimate goal is the translation to in vivo MRS to gain diagnostic and prognostic information non-invasively. 18F-fluorodeoxyglucose PET, an imaging modality often used in solid cancers of other organ systems, is not feasible, as the Warburg effect with increased glucose uptake is not present in prostate cancer, except for more advanced cases.[72,73,75,110] In vivo MRS can, at present, acquire metabolomic profiles per 0.5 cm^3 voxels in clinically feasible measurement time.[111–113] To meaningfully interpret the spectra in vivo, studies that correlate ex vivo spectroscopic data directly to histopathological features, as in the work presented here, are indispensable. Spectroscopic findings in the prostate from ex vivo studies are translatable to in vivo, as shown by a study that found a strong correlation between GS and the ratio (choline + creatine + spermine)/citrate both in vivo and ex vivo.[42]

We recommend (1) taking the next steps toward validation studies and, if successful, ultimately toward translation into the clinical workflow as a complementary ex vivo tool for bioptic prostate cancer detection and assessment of aggressiveness; (2) including the concept of field effects as a possible confounding factor in metabolomic study designs and data analysis; and (3) exploring field effects in other organ systems because there may be implications for both scientific and clinical applications as well.

5. References

1. Robert Koch-Gesellschaft & Gesellschaft der epidemiologischen Krebsregister in Deutschland e.V. *Krebs in Deutschland 2015/2016*. (2019).
2. Litwin, Mark S. & Tan, Hung-Jui. The diagnosis and treatment of prostate cancer: a review. *Jama* **317**, 2532–2542 (2017).
3. Leitlinienprogramm Onkologie (Arbeitsgemeinschaft der Wissenschaftlichen Medizinischen Fachgesellschaften e.V. (AWMF) & Deutschen Krebsgesellschaft e.V. (DKG) & Deutschen Krebshilfe (DKH)). *Interdisziplinäre Leitlinie der Qualität S3 zur Früherkennung, Diagnose und Therapie der verschiedenen Stadien des Prostatakarzinoms. Langversion 5.1* (2019).
4. Streicher, Justin, Meyerson, Brian Lee, Karivedu, Vidhya & Sidana, Abhinav. A review of optimal prostate biopsy: indications and techniques. *Ther. Adv. Urol.* **11**, 1756287219870074 (2019).
5. Wegelin, Olivier, van Melick, Harm H. E., Hooft, Lotty, Bosch, J. L. H. Ruud, Reitsma, Hans B., Barentsz, Jelle O. & Somford, Diederik M. Comparing three different techniques for magnetic resonance imaging-targeted prostate biopsies: a systematic review of in-bore versus magnetic resonance imaging-transrectal ultrasound fusion versus cognitive registration. Is there a preferred technique? *Eur. Urol.* **71**, 517–531 (2017).
6. Bjurlin, Marc A., Carter, H. Ballentine, Schellhammer, Paul, Cookson, Michael S., Gomella, Leonard G., Troyer, Dean, Wheeler, Thomas M., Schlossberg, Steven, Penson, David F. & Taneja, Samir S. Optimization of initial prostate biopsy in clinical practice: sampling, labeling and specimen processing. *J. Urol.* **189**, 2039–2046 (2013).
7. Andreoiu, Matei & Cheng, Liang. Multifocal prostate cancer: biologic, prognostic, and therapeutic implications. *Hum. Pathol.* **41**, 781–793 (2010).
8. Sved, Paul D., Gomez, Pablo, Manoharan, Murugesan, Kim, Sandy S. & Soloway, Mark S. Limitations of biopsy Gleason grade: implications for counseling patients with biopsy Gleason score 6 prostate cancer. *J. Urol.* **172**, 98–102 (2004).
9. Corcoran, Niall M., Hovens, Chris M., Hong, Matthew K. H., Pedersen, John, Casey, Rowan G., Connolly, Stephen, Peters, Justin, Harewood, Laurence, Gleave, Martin E. & Goldenberg, S. Larry. Underestimation of Gleason score at prostate biopsy reflects sampling error in lower volume tumours. *BJU Int.* **109**, 660–664 (2012).
10. Ahmed, Hashim U., Bosaily, Ahmed El-Shater, Brown, Louise C., Gabe, Rhian, Kaplan, Richard, Parmar, Mahesh K., Collaco-Moraes, Yolanda, Ward, Katie, Hindley, Richard G. & Freeman, Alex. Diagnostic accuracy of multi-parametric MRI and TRUS biopsy in prostate cancer (PROMIS): a paired validating confirmatory study. *Lancet* **389**, 815–822 (2017).
11. Welch, H. Gilbert & Black, William C. Overdiagnosis in cancer. *J. Natl. Cancer Inst.* **102**, 605–613 (2010).
12. Kasivisvanathan, Veeru, Rannikko, Antti S., Borghi, Marcelo, Panebianco, Valeria, Mynderse, Lance A., Vaarala, Markku H., Briganti, Alberto, Budäus, Lars, Hellawell, Giles & Hindley, Richard G. MRI-targeted or standard biopsy for prostate-cancer diagnosis. *N. Engl. J. Med.* **378**, 1767–1777 (2018).
13. Peltier, Alexandre, Aoun, Fouad, Lemort, Marc, Kwizera, Félix, Paesmans, Marianne & Van Velthoven, Roland. MRI-targeted biopsies versus systematic transrectal ultrasound guided biopsies for the diagnosis of localized prostate cancer in biopsy naïve men. *Biomed Res. Int.* **2015**, (2015).
14. Filson, Christopher P., Natarajan, Shyam, Margolis, Daniel J. A., Huang, Jiaoti, Lieu, Patricia, Dorey, Frederick J., Reiter, Robert E. & Marks, Leonard S. Prostate cancer detection with magnetic resonance-ultrasound fusion biopsy: The role of systematic and

targeted biopsies. *Cancer* **122**, 884–892 (2016).

15. de Gorski, Arachk, Rouprêt, Morgan, Peyronnet, Benoit, Le Cossec, Chloé, Granger, Benjamin, Comperat, Eva, Cussenot, Olivier, Renard-Penna, Raphaële & Mozer, Pierre. Accuracy of magnetic resonance imaging/ultrasound fusion targeted biopsies to diagnose clinically significant prostate cancer in enlarged compared to smaller prostates. *J. Urol.* **194**, 669–673 (2015).
16. Force, U. S. Preventive Services Task. Screening for Prostate Cancer: US Preventive Services Task Force Recommendation Statement. *JAMA* **319**, 1901–1913 (2018).
17. Pinsky, Paul F., Crawford, E. David, Kramer, Barnett S., Andriole, Gerald L., Gelmann, Edward P., Grubb, Robert, Greenlee, Robert & Gohagan, John K. Repeat prostate biopsy in the prostate, lung, colorectal and ovarian cancer screening trial. *BJU Int.* **99**, 775–779 (2007).
18. Fowler, Floyd J., Barry, Michael J., Walker-Corkery, Beth, Caubet, Jean-Francois, Bates, David W., Lee, Jeong Min, Hauser, Alison & McNaughton-Collins, Mary. The impact of a suspicious prostate biopsy on patients' psychological, socio-behavioral, and medical care outcomes. *J. Gen. Intern. Med.* **21**, 715–721 (2006).
19. Heidenreich, Axel, Bastian, Patrick J., Bellmunt, Joaquim, Bolla, Michel, Joniau, Steven, van der Kwast, Theodor, Mason, Malcolm, Matveev, Vsevolod, Wiegel, Thomas & Zattoni, F. EAU guidelines on prostate cancer. Part 1: screening, diagnosis, and local treatment with curative intent—update 2013. *Eur. Urol.* **65**, 124–137 (2014).
20. Lindon, John C., Nicholson, Jeremy K. & Holmes, Elaine. *The handbook of metabonomics and metabolomics*. (Elsevier, 2011).
21. Alonso, Arnald, Marsal, Sara & JuliÃ, Antonio. Analytical Methods in Untargeted Metabolomics: State of the Art in 2015. *Front. Bioeng. Biotechnol.* **3**, 23 (2015).
22. Sussulini, Alessandra. *Metabolomics: from fundamentals to clinical applications*. vol. 965 (Springer, 2017).
23. Bjerrum, Jacob T. & Bjerrum. *Metabonomics*. (Springer, 2015).
24. Jentzmik, Florian, Stephan, Carsten, Lein, Michael, Miller, Kurt, Kamlage, Beate, Bethan, Bianca, Kristiansen, Glen & Jung, Klaus. Sarcosine in prostate cancer tissue is not a differential metabolite for prostate cancer aggressiveness and biochemical progression. *J. Urol.* **185**, 706–711 (2011).
25. Keshari, K. R., Tsachres, H., Iman, R., Delos Santos, L., Tabatabai, Z. L., Shinohara, K., Vigneron, D. B. & Kurhanewicz, J. Correlation of phospholipid metabolites with prostate cancer pathologic grade, proliferative status and surgical stage–impact of tissue environment. *NMR Biomed.* **24**, 691–699 (2011).
26. Dinges, Sarah S., Vandergrift, Lindsey A., Wu, Shulin, Berker, Yannick, Habbel, Piet, Taupitz, Matthias, Wu, Chin-Lee & Cheng, Leo L. Metabolomic prostate cancer fields in HRMAS MRS-profiled histologically benign tissue vary with cancer status and distance from cancer. *NMR Biomed.* e4038 (2019).
27. Kdadra, Marouane, Höckner, Sebastian, Leung, Hing, Kremer, Werner & Schiffer, Eric. Metabolomics biomarkers of prostate cancer: a systematic review. *Diagnostics* **9**, 21 (2019).
28. Dinges, Sarah S., Hohm, Annika, Vandergrift, Lindsey A., Nowak, Johannes, Habbel, Piet, Kaltashov, Igor A. & Cheng, Leo L. Cancer metabolomic markers in urine: evidence, techniques and recommendations. *Nat. Rev. Urol.* **16**, 339–362 (2019).
29. Sitter, Beathe, Bathen, Tone F., Tessem, May-Britt & Gribbestad, Ingrid S. High-resolution magic angle spinning (HR MAS) MR spectroscopy in metabolic characterization of human cancer. *Prog. Nucl. Magn. Reson. Spectrosc.* **54**, 239–254 (2009).
30. Beckonert, Olaf, Coen, Muireann, Keun, Hector C., Wang, Yulan, Ebbels, Timothy M. D., Holmes, Elaine, Lindon, John C. & Nicholson, Jeremy K. High-resolution magic-angle-spinning NMR spectroscopy for metabolic profiling of intact tissues. *Nat. Protoc.* **5**, 1019–

1032 (2010).

31. Cheng, Leo L., Lean, Cynthia L., Bogdanova, Anna, Wright Jr, S. Carter, Ackerman, Jerome L., Brady, Thomas J. & Garrido, Leoncio. Enhanced resolution of proton NMR spectra of malignant lymph nodes using magic-angle spinning. *Magn. Reson. Med.* **36**, 653–658 (1996).
32. Cheng, Leo L., Burns, Melissa A., Taylor, Jennifer L., He, Wenlei, Halpern, Elkan F., McDougal, W. Scott & Wu, Chin-Lee. Metabolic Characterization of Human Prostate Cancer with Tissue Magnetic Resonance Spectroscopy. *Cancer Res.* **65**, 3030 LP – 3034 (2005).
33. van Asten, Jack J. A., Cuijpers, Vincent, Hulsbergen-van de Kaa, Christina, Soede-Huijbregts, Claudia, Witjes, J. Alfred, Verhofstad, Albert & Heerschap, Arend. High resolution magic angle spinning NMR spectroscopy for metabolic assessment of cancer presence and Gleason score in human prostate needle biopsies. *Magn. Reson. Mater. Physics, Biol. Med.* **21**, 435–442 (2008).
34. Meller, Sebastian, Meyer, Hellmuth-A., Bethan, Bianca, Dietrich, Dimo, Maldonado, Sandra González, Lein, Michael, Montani, Matteo, Reszka, Regina, Schatz, Philipp & Peter, Erik. Integration of tissue metabolomics, transcriptomics and immunohistochemistry reveals ERG-and gleason score-specific metabolomic alterations in prostate cancer. *Oncotarget* **7**, 1421 (2016).
35. Huan, Tao, Troyer, Dean A. & Li, Liang. Metabolite analysis and histology on the exact same tissue: comprehensive metabolomic profiling and metabolic classification of prostate cancer. *Sci. Rep.* **6**, 32272 (2016).
36. Ren, Shancheng, Shao, Yaping, Zhao, Xinjie, Hong, Christopher S., Wang, Fubo, Lu, Xin, Li, Jia, Ye, Guozhu, Yan, Min & Zhuang, Zhengping. Integration of metabolomics and transcriptomics reveals major metabolic pathways and potential biomarker involved in prostate cancer. *Mol. Cell. Proteomics* **15**, 154–163 (2016).
37. Sreekumar, Arun, Poisson, Laila M., Rajendiran, Thekkelnaycke M., Khan, Amjad P., Cao, Qi, Yu, Jindan, Laxman, Bharathi, Mehra, Rohit, Lonigro, Robert J. & Li, Yong. Metabolomic profiles delineate potential role for sarcosine in prostate cancer progression. *Nature* **457**, 910–914 (2009).
38. McDunn, Jonathan E., Li, Zhen, Adam, Klaus-Peter, Neri, Bruce P., Wolfert, Robert L., Milburn, Michael V, Lotan, Yair & Wheeler, Thomas M. Metabolomic signatures of aggressive prostate cancer. *Prostate* **73**, 1547–1560 (2013).
39. Shuster, Jeffrey R., Lance, Raymond S. & Troyer, Dean A. Molecular preservation by extraction and fixation, mPREF: a method for small molecule biomarker analysis and histology on exactly the same tissue. *BMC Clin. Pathol.* **11**, 14 (2011).
40. Jung, Klaus, Reszka, Regina, Kamlage, Beate, Bethan, Bianca, Stephan, Carsten, Lein, Michael & Kristiansen, Glen. Tissue metabolite profiling identifies differentiating and prognostic biomarkers for prostate carcinoma. *Int. J. cancer* **133**, 2914–2924 (2013).
41. Giskeødegård, Guro F., Bertilsson, Helena, Selnæs, Kirsten M., Wright, Alan J., Bathen, Tone F., Viset, Trond, Halgunset, Jostein, Angelsen, Anders, Gribbestad, Ingrid S. & Tessem, May-Britt. Spermine and citrate as metabolic biomarkers for assessing prostate cancer aggressiveness. *PLoS One* **8**, e62375 (2013).
42. Selnæs, Kirsten M., Gribbestad, Ingrid S., Bertilsson, Helena, Wright, Alan, Angelsen, Anders, Heerschap, Arend & Tessem, May-Britt. Spatially matched in vivo and ex vivo MR metabolic profiles of prostate cancer–investigation of a correlation with Gleason score. *NMR Biomed.* **26**, 600–606 (2013).
43. Thysell, Elin, Surowiec, Izabella, Hörnberg, Emma, Crnalic, Sead, Widmark, Anders, Johansson, Annika I., Stattin, Pär, Bergh, Anders, Moritz, Thomas & Antti, Henrik. Metabolomic characterization of human prostate cancer bone metastases reveals increased

levels of cholesterol. *PLoS One* **5**, (2010).

44. Maxeiner, Andreas, Adkins, Christen B., Zhang, Yifen, Taupitz, Matthias, Halpern, Elkan F., McDougal, W. Scott, Wu, Chin-Lee & Cheng, Leo L. Retrospective analysis of prostate cancer recurrence potential with tissue metabolomic profiles. *Prostate* **70**, 710–717 (2010).
45. Slaughter, Danely P., Southwick, Harry W. & Smejkal, Walter. "Field cancerization" in oral stratified squamous epithelium. Clinical implications of multicentric origin. *Cancer* **6**, 963–968 (1953).
46. Trujillo, Kristina A., Jones, Anna C., Griffith, Jeffrey K. & Bisoffi, Marco. Markers of field cancerization: proposed clinical applications in prostate biopsies. *Prostate Cancer* **2012**, 302894 (2012).
47. Nonn, Larisa, Ananthanarayanan, Vijayalakshmi & Gann, Peter H. Evidence for field cancerization of the prostate. *Prostate* **69**, 1470–1479 (2009).
48. Stenman, Katarina, Stattin, Pär, Stenlund, Hans, Riklund, Katrine, Gröbner, Gerhard & Bergh, Anders. H HRMAS NMR Derived Bio-markers Related to Tumor Grade, Tumor Cell Fraction, and Cell Proliferation in Prostate Tissue Samples. *Biomark. Insights* **6**, BMI.S6794 (2011).
49. Jiménez, Beatriz, Mirnezami, Reza, Kinross, James, Cloarec, Olivier, Keun, Hector C., Holmes, Elaine, Goldin, Robert D., Ziprin, Paul, Darzi, Ara & Nicholson, Jeremy K. 1H HR-MAS NMR spectroscopy of tumor-induced local metabolic "field-effects" enables colorectal cancer staging and prognostication. *J. Proteome Res.* **12**, 959–968 (2013).
50. Reed, Michelle A. C., Singhal, Rishi, Ludwig, Christian, Carrigan, John B., Ward, Douglas G., Taniere, Phillipe, Alderson, Derek & Günther, Ulrich L. Metabolomic evidence for a field effect in histologically normal and metaplastic tissues in patients with esophageal adenocarcinoma. *Neoplasia* **19**, 165–174 (2017).
51. Yakoub, Danny, Keun, Hector C., Goldin, Robert & Hanna, George B. Metabolic profiling detects field effects in nondysplastic tissue from esophageal cancer patients. *Cancer Res.* **70**, 9129–9136 (2010).
52. Halin, Sofia, Hammarsten, Peter, Adamo, Hani, Wikström, Pernilla & Bergh, Anders. Tumor indicating normal tissue could be a new source of diagnostic and prognostic markers for prostate cancer. *Expert Opin. Med. Diagn.* **5**, 37–47 (2011).
53. Curtius, Kit, Wright, Nicholas A. & Graham, Trevor A. An evolutionary perspective on field cancerization. *Nat. Rev. Cancer* **18**, 19 (2018).
54. Rybicki, Benjamin A., Rundle, Andrew, Kryvenko, Oleksandr N., Mitrache, Nicoleta, Do, Kieu C., Jankowski, Michelle, Chitale, Dhananjay A., Trudeau, Sheri, Belinsky, Steven A. & Tang, Deliang. Methylation in benign prostate and risk of disease progression in men subsequently diagnosed with prostate cancer. *Int. J. cancer* **138**, 2884–2893 (2016).
55. Vandergrift, Lindsey A., Decelle, Emily A., Kurth, Johannes, Wu, Shulin, Fuss, Taylor L., DeFeo, Elita M., Halpern, Elkan F., Taupitz, Matthias, McDougal, W. Scott & Olumi, Aria F. Metabolomic prediction of human prostate cancer aggressiveness: magnetic resonance spectroscopy of histologically benign tissue. *Sci. Rep.* **8**, 4997 (2018).
56. Epstein, Jonathan I., Zelefsky, Michael J., Sjoberg, Daniel D., Nelson, Joel B., Egevad, Lars, Magi-Galluzzi, Cristina, Vickers, Andrew J., Parwani, Anil V, Reuter, Victor E. & Fine, Samson W. A contemporary prostate cancer grading system: a validated alternative to the Gleason score. *Eur. Urol.* **69**, 428–435 (2016).
57. Haukaas, Tonje H., Moestue, Siver A., Vettukattil, Riyas, Sitter, Beathe, Lamichhane, Santosh, Segura, Remedios, Giskeødegård, Guro F. & Bathen, Tone F. Impact of freezing delay time on tissue samples for metabolomic studies. *Front. Oncol.* **6**, 17 (2016).
58. Paner Gladell P, R, Srigley John, Ming, Zhou, Allan, Robert, Amin, Mahul B. Amin, Chang, Sam S., Delahunt, Brett, Egevad, Lars, Epstein, Jonathan I., Evans, Andrew J., Grignon, David J., Humphrey, Peter A., McKiernan, James M., Montironi, Rodolfo, Pettus, Jason,

Reuter, Victor E. & Wheeler, Thomas M. *Protocol for the Examination of Specimens From Patients With Carcinoma of the Prostate Gland.* https://documents.cap.org/protocols/cp-malegenital-prostate-18protocol-4030.pdf (2017).

59. Jordan, Kate W., He, Wenlei, Halpern, Elkan F., Wu, Chin-Lee & Cheng, Leo L. Evaluation of tissue metabolites with high resolution magic angle spinning MR spectroscopy human prostate samples after three-year storage at–80 C. *Biomark. Insights* **2**, 117727190700200000 (2007).
60. Burns, Melissa A., Taylor, Jennifer L., Wu, Chin-Lee, Zepeda, Andrea G., Bielecki, Anthony, Cory, David & Cheng, Leo L. Reduction of spinning sidebands in proton NMR of human prostate tissue with slow high-resolution magic angle spinning. *Magn. Reson. Med. An Off. J. Int. Soc. Magn. Reson. Med.* **54**, 34–42 (2005).
61. Taylor, Jennifer L., Wu, Chin-Lee, Cory, David, Gonzalez, R. Gilberto, Bielecki, Anthony & Cheng, Leo L. High-resolution magic angle spinning proton NMR analysis of human prostate tissue with slow spinning rates. *Magn. Reson. Med. An Off. J. Int. Soc. Magn. Reson. Med.* **50**, 627–632 (2003).
62. Schneider, Caroline A., Rasband, Wayne S. & Eliceiri, Kevin W. NIH Image to ImageJ: 25 years of image analysis. *Nat. Methods* **9**, 671 (2012).
63. van den Berg, Robert A., Hoefsloot, Huub C. J., Westerhuis, Johan A., Smilde, Age K. & van der Werf, Mariet J. Centering, scaling, and transformations: improving the biological information content of metabolomics data. *BMC Genomics* **7**, 142 (2006).
64. Breiman, Leo & Cutler, Adele. Random Forests. https://www.stat.berkeley.edu/~breiman/RandomForests/cc_home.htm#micro7.
65. Worley, Bradley & Powers, Robert. Multivariate analysis in metabolomics. *Curr. Metabolomics* **1**, 92–107 (2013).
66. Saccenti, Edoardo, Hoefsloot, Huub C. J., Smilde, Age K., Westerhuis, Johan A. & Hendriks, Margriet M. W. B. Reflections on univariate and multivariate analysis of metabolomics data. *Metabolomics* **10**, 361–374 (2014).
67. Thévenot, Etienne A., Roux, Aurélie, Xu, Ying, Ezan, Eric & Junot, Christophe. Analysis of the human adult urinary metabolome variations with age, body mass index, and gender by implementing a comprehensive workflow for univariate and OPLS statistical analyses. *J. Proteome Res.* **14**, 3322–3335 (2015).
68. Wishart, David S., Tzur, Dan, Knox, Craig, Eisner, Roman, Guo, An Chi, Young, Nelson, Cheng, Dean, Jewell, Kevin, Arndt, David & Sawhney, Summit. HMDB: the human metabolome database. *Nucleic Acids Res.* **35**, D521–D526 (2007).
69. Kanehisa, Minoru. The KEGG database. in *Novartis Foundation Symposium* 91–100 (Wiley Online Library, 2002).
70. Xia, Jianguo & Wishart, David S. Web-based inference of biological patterns, functions and pathways from metabolomic data using MetaboAnalyst. *Nat. Protoc.* **6**, 743 (2011).
71. R Foundation for Statistical Computing. R: A language and environment for statistical computing. https://www.r-project.org/ (2018).
72. Mah, Chui Yan, Nassar, Zeyad D., Swinnen, Johannes V & Butler, Lisa M. Lipogenic effects of androgen signaling in normal and malignant prostate. *Asian J. Urol.* (2019).
73. Costello, Leslie C. & Franklin, Renty B. The clinical relevance of the metabolism of prostate cancer; zinc and tumor suppression: connecting the dots. *Mol. Cancer* **5**, 17 (2006).
74. Roberts, Matthew J., Schirra, Horst Joachim, Lavin, Martin F. & Gardiner, Robert A. NMR-based metabolomics: global analysis of metabolites to address problems in prostate cancer. *Cervical, Breast and Prostate Cancer* 1–43 (2014).
75. Eidelman, Eric, Twum-Ampofo, Jeffrey, Ansari, Jamal & Siddiqui, Mohummad Minhaj. The metabolic phenotype of prostate cancer. *Front. Oncol.* **7**, 131 (2017).
76. Amamoto, Rie, Uchiumi, Takeshi, Yagi, Mikako, Monji, Keisuke, Song, YooHyun, Oda,

Yoshinao, Shiota, Masaki, Yokomizo, Akira, Naito, Seiji & Kang, Dongchon. The expression of ubiquitous mitochondrial creatine kinase is downregulated as prostate cancer progression. *J. Cancer* **7**, 50 (2016).

77. Zhang, V. Y., Westphalen, A., Delos Santos, L., Tabatabai, Z. L., Shinohara, K., Vigneron, D. B. & Kurhanewicz, J. The role of metabolic imaging in radiation therapy of prostate cancer. *NMR Biomed.* **27**, 100–111 (2014).
78. Vettore, Lisa, Westbrook, Rebecca L. & Tennant, Daniel A. New aspects of amino acid metabolism in cancer. *Br. J. Cancer* **122**, 150–156 (2020).
79. Zadra, Giorgia, Photopoulos, Cornelia & Loda, Massimo. The fat side of prostate cancer. *Biochim. Biophys. Acta (BBA)-Molecular Cell Biol. Lipids* **1831**, 1518–1532 (2013).
80. Andersen, Maria K., Høiem, Therese S., Claes, Britt S. R., Balluff, Benjamin, Martin-Lorenzo, Marta, Richardsen, Elin, Krossa, Sebastian, Bertilsson, Helena, Heeren, Ron M. A. & Rye, Morten B. Spatial differentiation of metabolism in prostate cancer tissue by MALDI-TOF MSI. *Cancer Metab.* **9**, 1–13 (2021).
81. Randall, Elizabeth C., Zadra, Giorgia, Chetta, Paolo, Lopez, Begona G. C., Syamala, Sudeepa, Basu, Sankha S., Agar, Jeffrey N., Loda, Massimo, Tempany, Clare M. & Fennessy, Fiona M. Molecular characterization of prostate cancer with associated Gleason score using mass spectrometry imaging. *Mol. Cancer Res.* **17**, 1155–1165 (2019).
82. Valentino, A., Calarco, A., Di Salle, A., Finicelli, M., Crispi, S., Calogero, Raffaele Adolfo, Riccardo, F., Sciarra, A., Gentilucci, A. & Galderisi, U. Deregulation of MicroRNAs mediated control of carnitine cycle in prostate cancer: molecular basis and pathophysiological consequences. *Oncogene* **36**, 6030–6040 (2017).
83. DeGrado, Timothy R., Coleman, R. Edward, Wang, Shuyan, Baldwin, Steven W., Orr, Matthew D., Robertson, Cary N., Polascik, Thomas J. & Price, David T. Synthesis and evaluation of 18F-labeled choline as an oncologic tracer for positron emission tomography: initial findings in prostate cancer. *Cancer Res.* **61**, 110–117 (2001).
84. Ackerstaff, Ellen, Glunde, Kristine & Bhujwalla, Zaver M. Choline phospholipid metabolism: a target in cancer cells? *J. Cell. Biochem.* **90**, 525–533 (2003).
85. Swanson, Mark G., Vigneron, Daniel B., Tabatabai, Z. Laura, Males, Ryan G., Schmitt, Lars, Carroll, Peter R., James, Joyce K., Hurd, Ralph E. & Kurhanewicz, John. Proton HR-MAS spectroscopy and quantitative pathologic analysis of MRI/3D-MRSI-targeted postsurgical prostate tissues. *Magn. Reson. Med. An Off. J. Int. Soc. Magn. Reson. Med.* **50**, 944–954 (2003).
86. Swanson, Mark G., Zektzer, Andrew S., Tabatabai, Z. Laura, Simko, Jeffry, Jarso, Samson, Keshari, Kayvan R., Schmitt, Lars, Carroll, Peter R., Shinohara, Katsuto & Vigneron, Daniel B. Quantitative analysis of prostate metabolites using 1H HR-MAS spectroscopy. *Magn. Reson. Med. An Off. J. Int. Soc. Magn. Reson. Med.* **55**, 1257–1264 (2006).
87. Lou, Tzu-Fang, Sethuraman, Deepa, Dospoy, Patrick, Srivastva, Pallevi, Kim, Hyun Seok, Kim, Joongsoo, Ma, Xiaotu, Chen, Pei-Hsuan, Huffman, Kenneth E. & Frink, Robin E. Cancer-specific production of N-acetylaspartate via NAT8L overexpression in non–small cell lung cancer and its potential as a circulating biomarker. *Cancer Prev. Res.* **9**, 43–52 (2016).
88. Tayari, Nassim, Heerschap, Arend, Scheenen, Tom W. J. & Kobus, Thiele. In vivo MR spectroscopic imaging of the prostate, from application to interpretation. *Anal. Biochem.* **529**, 158–170 (2017).
89. Casero, Robert A., Stewart, Tracy Murray & Pegg, Anthony E. Polyamine metabolism and cancer: treatments, challenges and opportunities. *Nat. Rev. Cancer* **18**, 681–695 (2018).
90. Cheng, Leo Ling, Wu, Chin-lee, Smith, Matthew R. & Gonzalez, R. Gilberto. Non-destructive quantitation of spermine in human prostate tissue samples using HRMAS 1H NMR spectroscopy at 9.4 T. *FEBS Lett.* **494**, 112–116 (2001).

91. Griffin, Julian L. & Shockcor, John P. Metabolic profiles of cancer cells. *Nat. Rev. cancer* **4**, 551–561 (2004).
92. Baliou, Stella, Kyriakopoulos, Anthony M., Spandidos, Demetrios A. & Zoumpourlis, Vassilios. Role of taurine, its haloamines and its lncRNA TUG1 in both inflammation and cancer progression. On the road to therapeutics? *Int. J. Oncol.* **57**, 631–664 (2020).
93. Hahn, Per, Smith, Ian C. P., Leboldus, Leonard, Littman, Charles, Somorjai, Ray L. & Bezabeh, Tedros. The classification of benign and malignant human prostate tissue by multivariate analysis of 1H magnetic resonance spectra. *Cancer Res.* **57**, 3398–3401 (1997).
94. Tessem, May-Britt, Bertilsson, Helena, Angelsen, Anders, Bathen, Tone F., Drabløs, Finn & Rye, Morten Beck. A balanced tissue composition reveals new metabolic and gene expression markers in prostate cancer. *PLoS One* **11**, e0153727 (2016).
95. Schad, Martina, Mungur, Rajsree, Fiehn, Oliver & Kehr, Julia. Metabolic profiling of laser microdissected vascular bundles of Arabidopsis thaliana. *Plant Methods* **1**, 2 (2005).
96. Eberlin, Livia S., Liu, Xiaohui, Ferreira, Christina R., Santagata, Sandro, Agar, Nathalie Y. R. & Cooks, R. Graham. Desorption electrospray ionization then MALDI mass spectrometry imaging of lipid and protein distributions in single tissue sections. *Anal. Chem.* **83**, 8366–8371 (2011).
97. Bourne, Roger. Re: Metabolomic prostate cancer fields in HRMAS MRS-profiled histologically benign tissue vary with cancer status and distance from cancer. Dinges et al, NBM 2019. *NMR Biomed.* **32**, e4121 (2019).
98. Tuxhorn, Jennifer A., Ayala, Gustavo E., Smith, Megan J., Smith, Vincent C., Dang, Truong D. & Rowley, David R. Reactive Stroma in Human Prostate Cancer. *Clin. Cancer Res.* **8**, 2912 LP – 2923 (2002).
99. Andersen, Maria K., Rise, Kjersti, Giskeødegård, Guro F., Richardsen, Elin, Bertilsson, Helena, Størkersen, Øystein, Bathen, Tone F., Rye, Morten & Tessem, May-Britt. Integrative metabolic and transcriptomic profiling of prostate cancer tissue containing reactive stroma. *Sci. Rep.* **8**, 14269 (2018).
100. Soto, Ana M. & Sonnenschein, Carlos. The tissue organization field theory of cancer: a testable replacement for the somatic mutation theory. *Bioessays* **33**, 332–340 (2011).
101. Hansen, Ailin Falkmo, Sandsmark, Elise, Rye, Morten Beck, Wright, Alan J., Bertilsson, Helena, Richardsen, Elin, Viset, Trond, Bofin, Anna M., Angelsen, Anders & Selnæs, Kirsten M. Presence of TMPRSS2-ERG is associated with alterations of the metabolic profile in human prostate cancer. *Oncotarget* **7**, 42071 (2016).
102. Liu, Wei, Bai, Xuefeng, Liu, Yuejuan, Wang, Wei, Han, Junwei, Wang, Qiuyu, Xu, Yanjun, Zhang, Chunlong, Zhang, Shihua & Li, Xuecang. Topologically inferring pathway activity toward precise cancer classification via integrating genomic and metabolomic data: prostate cancer as a case. *Sci. Rep.* **5**, 13192 (2015).
103. Sandsmark, Elise, Hansen, Ailin Falkmo, Selnæs, Kirsten M., Bertilsson, Helena, Bofin, Anna M., Wright, Alan J., Viset, Trond, Richardsen, Elin, Drabløs, Finn & Bathen, Tone F. A novel non-canonical Wnt signature for prostate cancer aggressiveness. *Oncotarget* **8**, 9572 (2017).
104. Gordetsky, Jennifer & Epstein, Jonathan. Grading of prostatic adenocarcinoma: current state and prognostic implications. *Diagn. Pathol.* **11**, 25 (2016).
105. Maruthi Padmaja, T., Raju, Bapi S., Hota, Rudra N. & Krishna, P. Radha. Class imbalance and its effect on PCA preprocessing. *Int. J. Knowl. Eng. Soft Data Paradig.* **4**, 272–294 (2014).
106. Tolkach, Yuri, Thomann, Stefan & Kristiansen, Glen. Three-dimensional reconstruction of prostate cancer architecture with serial immunohistochemical sections: hallmarks of tumour growth, tumour compartmentalisation, and implications for grading and heterogeneity. *Histopathology* **72**, 1051–1059 (2018).

107. Salek, Reza M., Haug, Kenneth & Steinbeck, Christoph. Dissemination of metabolomics results: role of MetaboLights and COSMOS. *Gigascience* **2**, 8 (2013).
108. Wanichthanarak, Kwanjeera, Jeamsripong, Saharuetai, Pornputtapong, Natapol & Khoomrung, Sakda. Accounting for biological variation with linear mixed-effects modelling improves the quality of clinical metabolomics data. *Comput. Struct. Biotechnol. J.* **17**, 611–618 (2019).
109. Pinu, Farhana R., Goldansaz, Seyed Ali & Jaine, Jacob. Translational Metabolomics: Current Challenges and Future Opportunities. *Metabolites* **9**, 108 (2019).
110. Scroggins, Bradley T., Matsuo, Masayuki, White, Ayla O., Saito, Keita, Munasinghe, Jeeva P., Sourbier, Carole, Yamamoto, Kazutoshi, Diaz, Vivian, Takakusagi, Yoichi & Ichikawa, Kazuhiro. Hyperpolarized [1-13C]-pyruvate magnetic resonance spectroscopic imaging of prostate cancer in vivo predicts efficacy of targeting the Warburg effect. *Clin. Cancer Res.* **24**, 3137–3148 (2018).
111. Tayari, Nassim, Heerschap, Arend, Scheenen, Tom W. J. & Kobus, Thiele. In vivo MR spectroscopic imaging of the prostate, from application to interpretation. *Anal. Biochem.* **529**, 158–170 (2017).
112. Kobus, Thiele, Vos, Pieter C., Hambrock, Thomas, De Rooij, Maarten, Hulsbergen—Van de Kaa, Christina A., Barentsz, Jelle O., Heerschap, Arend & Scheenen, Tom W. J. Prostate Cancer Aggressiveness: In Vivo Assessment of MR Spectroscopy and Diffusion-weighted Imaging at 3 T. *Radiology* **265**, 457–467 (2012).
113. Verma, Sadhna, Rajesh, Arumugam, Fütterer, Jurgen J., Turkbey, Baris, Scheenen, Tom W. J., Pang, Yuxi, Choyke, Peter L. & Kurhanewicz, John. Prostate MRI and 3D MR spectroscopy: how we do it. *AJR. Am. J. Roentgenol.* **194**, 1414–1426 (2010).

Eidesstattliche Versicherung

„Ich, Sarah Svenja Dinges, versichere an Eides statt durch meine eigenhändige Unterschrift, dass ich die vorgelegte Dissertation mit dem Thema: The Diagnostic Potential of Metabolomic Prostate Cancer Field Effects (Das diagnostische Potential von metabolomischen Effekten in der Tumorumgebung bei Prostatakrebs) selbstständig und ohne nicht offengelegte Hilfe Dritter verfasst und keine anderen als die angegebenen Quellen und Hilfsmittel genutzt habe.

Alle Stellen, die wörtlich oder dem Sinne nach auf Publikationen oder Vorträgen anderer Autoren/innen beruhen, sind als solche in korrekter Zitierung kenntlich gemacht. Die Abschnitte zu Methodik (insbesondere praktische Arbeiten, Laborbestimmungen, statistische Aufarbeitung) und Resultaten (insbesondere Abbildungen, Graphiken und Tabellen) werden von mir verantwortet.

Ich versichere ferner, dass ich die in Zusammenarbeit mit anderen Personen generierten Daten, Datenauswertungen und Schlussfolgerungen korrekt gekennzeichnet und meinen eigenen Beitrag sowie die Beiträge anderer Personen korrekt kenntlich gemacht habe (siehe Anteilserklärung). Texte oder Textteile, die gemeinsam mit anderen erstellt oder verwendet wurden, habe ich korrekt kenntlich gemacht.

Meine Anteile an etwaigen Publikationen zu dieser Dissertation entsprechen denen, die in der untenstehenden gemeinsamen Erklärung mit dem Erstbetreuer, angegeben sind. Für sämtliche im Rahmen der Dissertation entstandenen Publikationen wurden die Richtlinien des ICMJE (International Committee of Medical Journal Editors; www.icmje.og) zur Autorenschaft eingehalten. Ich erkläre ferner, dass ich mich zur Einhaltung der Satzung der Charité – Universitätsmedizin Berlin zur Sicherung Guter Wissenschaftlicher Praxis verpflichte.

Weiterhin versichere ich, dass ich diese Dissertation weder in gleicher noch in ähnlicher Form bereits an einer anderen Fakultät eingereicht habe.

Die Bedeutung dieser eidesstattlichen Versicherung und die strafrechtlichen Folgen einer unwahren eidesstattlichen Versicherung (§§156, 161 des Strafgesetzbuches) sind mir bekannt und bewusst.“

____________________________ ____________________________

Ort, Datum Unterschrift

Ausführliche Anteilserklärung an der Publikation zur Top-Journal Dissertation

Publikation: Dinges, Sarah S., Vandergrift, Lindsey A., Wu, Shulin, Berker, Yannick, Habbel, Piet, Taupitz, Matthias, Wu, Chin-Lee, Cheng & Leo L. Metabolomic prostate cancer fields in HRMAS MRS-profiled histologically benign tissue vary with cancer status and distance from cancer. NMR in biomedicine 32(10):e4038 (2019).

Beitrag im Einzelnen:

Ich, **Sarah S. Dinges**, war maßgeblich beteiligt an Studiendesign, -koordination und -organisation. Im Rahmen des Projektes habe ich Kooperationen zwischen meiner Arbeitsgruppe und der statistischen sowie der pathologischen Abteilung etabliert. Im Speziellen habe ich die Organe aus dem Operationssaal entgegengenommen und das pathologische Schneiden zusammen mit Chin-Lee Wu durchgeführt. Ich habe selbstständig die Gewebeproben aufbereitet, die spektroskopischen Messungen durchgeführt und die Rohdaten verarbeitet. Ich habe das Gewebe histopathologisch geschnitten und gefärbt und gemeinsam mit Shulin Wu sämtliche Schnitte lichtmikroskopisch ausgelesen. Ich habe eigenständig die klinischen Daten zusammengetragen, Programme zur weiteren Aufbereitung der präprozessierten spektroskopischen Daten geschrieben und anschließend die statistische Auswertung durchgeführt. Ich habe die Literaturrecherche zum Konzept *field cancerization* und insbesondere zu metabolomischen Messungen in histologisch benignem Gewebe vorgenommen. Ich habe das Manuskript verfasst und sämtliche Visualisierungen und Tabellen erstellt, die den Forschungsbereich field cancerization, also Messungen in histologisch benignem Gewebe, und die Primärforschung betreffen. Das heißt, von mir erstellt wurden sämtliche Abbildungen, Tabellen (außer Tabelle 1) und Textteile (außer 1.1, 1.1.1 und 1.2 Absatz eins und zwei bis einschließlich "[...] there has been increasing establishment of automated MRS facilities attached to surgical theaters."). Aus Gründen der Übersichtlichkeit verzichte ich auf eine Auflistung der auf meine Arbeit zurückgehenden Abbildungen, Tabellen und Textteile und belasse es bei der Darstellung der Ausnahmen, die nur einen kleinen Teil der Publikation ausmachen.

Lindsey A. Vandergrift, Labortechnikerin der Arbeitsgruppe, hat mir die praktischen Fähigkeiten zur Bedienung des Spektrometers, der Programme zum Prozessieren der spektroskopischen Rohdaten und zum histopathologischen Aufbereiten der Gewebeproben vermittelt. Für die oben genannte Publikation hat sie die Literaturrecherche zu metabolomischen Messungen in Krebsgewebe im Allgemeinen durchgeführt. Die Ergebnisse dieser Literaturrecherche hat Frau Vandergrift in einer Tabelle und einigen Absätzen dargestellt:

- **Table 1 Selected HRMAS MRS metabolomic studies within the past 10 year**
- **1.1 | The current state of HRMAS MRS- based human cancer metabolomics**
- **1.1.1 | Methodological considerations**
- **1.2 | Fields of investigation and clinical applications**; hier gehen die ersten beiden Absätze auf Frau Vandergrift zurück (bis einschließlich "[...] there has been increasing establishment of automated MRS facilities attached to surgical theaters.")

Chin-Lee Wu war maßgeblich verantwortlich für das pathologische Schneiden der Organe und **Shulin Wu** hat die histopathologischen Proben ausgelesen, wobei ich bei beiden Arbeitsschritten stets anwesend war und mitgewirkt habe. **Yannick Berker** hat die Programme zur Prozessierung der spektroskopischen Rohdaten geschrieben und bei der statistischen Auswertung der Daten geholfen. **Matthias Taupitz** und **Piet Habbel** haben maßgeblich an Organisation und inhaltlicher Gestaltung der Arbeit mitgewirkt. Auf **Leo L. Cheng** als Letztautor und Leiter der Arbeitsgruppe sind die Idee zu der Arbeit sowie ihre Finanzierung und Koordination zurückzuführen.

Journal Data Filtered By: **Selected JCR Year: 2016** Selected Editions: SCIE,SSCI Selected Categories: **“RADIOLOGY, NUCLEAR MEDICINE and MEDICAL IMAGING”** Selected Category Scheme: WoS

Gesamtanzahl: 126 Journale

Rank	Full Journal Title	Total Cites	Journal Impact Factor	Eigenfactor Score
1	JACC-Cardiovascular Imaging	6,895	10.189	0.027050
2	RADIOLOGY	50,983	7.296	0.066140
3	EUROPEAN JOURNAL OF NUCLEAR MEDICINE AND MOLECULAR IMAGING	14,019	7.277	0.024910
4	Circulation-Cardiovascular Imaging	4,472	6.803	0.019120
5	JOURNAL OF NUCLEAR MEDICINE	24,977	6.646	0.037540
6	NEUROIMAGE	85,630	5.835	0.173210
7	JOURNAL OF CARDIOVASCULAR MAGNETIC RESONANCE	4,349	5.601	0.014950
8	SEMINARS IN RADIATION ONCOLOGY	2,232	5.356	0.003910
9	INVESTIGATIVE RADIOLOGY	5,925	5.195	0.011230
10	INTERNATIONAL JOURNAL OF RADIATION ONCOLOGY BIOLOGY PHYSICS	44,068	5.133	0.060060
11	ULTRASOUND IN OBSTETRICS & GYNECOLOGY	11,611	4.710	0.019350
12	HUMAN BRAIN MAPPING	18,139	4.530	0.041900
13	RADIOTHERAPY AND ONCOLOGY	15,639	4.328	0.028040
14	MEDICAL IMAGE ANALYSIS	5,539	4.188	0.010720
15	EUROPEAN RADIOLOGY	16,381	3.967	0.033340
16	IEEE TRANSACTIONS ON MEDICAL IMAGING	15,215	3.942	0.019660
17	JOURNAL OF NUCLEAR CARDIOLOGY	3,021	3.930	0.003920
18	MAGNETIC RESONANCE IN MEDICINE	29,816	3.924	0.035960
19	CLINICAL NUCLEAR MEDICINE	4,008	3.640	0.006470
20	SEMINARS IN NUCLEAR MEDICINE	2,056	3.630	0.002800
21	AMERICAN JOURNAL OF NEURORADIOLOGY	21,720	3.550	0.032180
22	MOLECULAR IMAGING AND BIOLOGY	2,228	3.466	0.005880
23	ULTRASCHALL IN DER MEDIZIN	1,907	3.452	0.003930
24	RADIOGRAPHICS	10,286	3.427	0.009660
25	Biomedical Optics Express	6,187	3.337	0.021610
26	Contrast Media & Molecular Imaging	1,131	3.307	0.002810
27	INTERNATIONAL JOURNAL OF HYPERTHERMIA	3,030	3.262	0.003810

Rank	Full Journal Title	Total Cites	Journal Impact Factor	Eigenfactor Score
28	Journal of Cardiovascular Computed Tomography	1,331	3.185	0.004220
29	JOURNAL OF MAGNETIC RESONANCE IMAGING	15,073	3.083	0.029170
30	Journal of the American College of Radiology	2,690	2.993	0.006840
31	NMR IN BIOMEDICINE	6,766	2.872	0.014560
32	JOURNAL OF VASCULAR AND INTERVENTIONAL RADIOLOGY	8,371	2.780	0.012840
33	AMERICAN JOURNAL OF ROENTGENOLOGY	31,676	2.778	0.035740
34	PHYSICS IN MEDICINE AND BIOLOGY	22,873	2.742	0.034390
35	STRAHLENTHERAPIE UND ONKOLOGIE	2,687	2.735	0.004990
36	Clinical Neuroradiology	433	2.618	0.001550
37	MEDICAL PHYSICS	22,942	2.617	0.037250
38	Radiation Oncology	4,358	2.568	0.013680
39	RADIATION RESEARCH	8,394	2.539	0.007920
40	JOURNAL OF BIOMEDICAL OPTICS	12,700	2.530	0.024520
41	JOURNAL OF NEURORADIOLOGY	792	2.526	0.001310
42	ULTRASOUND IN MEDICINE AND BIOLOGY	9,759	2.494	0.012640
43	QUARTERLY JOURNAL OF NUCLEAR MEDICINE AND MOLECULAR IMAGING	1,030	2.481	0.001800
44	CLINICAL RADIOLOGY	5,717	2.478	0.008540
45	EUROPEAN JOURNAL OF RADIOLOGY	11,328	2.462	0.026500
46	NUCLEAR MEDICINE AND BIOLOGY	3,918	2.426	0.006210
47	CANCER IMAGING	1,008	2.404	0.001930
48	RADIATION AND ENVIRONMENTAL BIOPHYSICS	1,468	2.398	0.002460
49	ULTRASONICS	5,752	2.327	0.008130
50	Diagnostic and Interventional Imaging	957	2.277	0.002420
51	MAGNETIC RESONANCE IMAGING	6,465	2.225	0.011370
52	CARDIOVASCULAR AND INTERVENTIONAL RADIOLOGY	4,859	2.191	0.008890
53	KOREAN JOURNAL OF RADIOLOGY	1,941	2.156	0.003730
54	ACADEMIC RADIOLOGY	4,804	2.128	0.009150
55	NEURORADIOLOGY	5,191	2.093	0.007520
56	Dose-Response	671	2.088	0.001310
57	Brachytherapy	1,442	2.082	0.003540
58	BRITISH JOURNAL OF RADIOLOGY	7,990	2.050	0.011760
59	EJNMMI Research	844	2.033	0.003380

Die im Folgenden genannte Publikation wird aus datenschutzrechtlichen Gründen in der elektronischen Version meiner Arbeit nicht veröffentlicht.

Dinges, Sarah S., Vandergrift, Lindsey A., Wu, Shulin, Berker, Yannick, Habbel, Piet, Taupitz, Matthias, Wu, Chin-Lee & Cheng, Leo L. Metabolomic prostate cancer fields in HRMAS MRS-profiled histologically benign tissue vary with cancer status and distance from cancer. NMR Biomed. e4038 (2019).

https://doi.org/10.1002/nbm.4038

Lebenslauf Sarah S. Dinges

Mein Mein Lebenslauf wird aus datenschutzrechtlichen Gründen in der elektronischen Version meiner Arbeit nicht veröffentlicht.

Publikationsliste Sarah S. Dinges

Stand: 06.06.2021

Dinges, Sarah S., Hohm, Annika, Vandergrift, Lindsey A., Nowak, Johannes, Habbel, Piet, Kaltashov, Igor A. & Cheng, Leo L. **Cancer metabolomic markers in urine: evidence, techniques and recommendations.** *Nat. Rev. Urol.* 16, 339–362 (2019).

Dinges, Sarah S., Vandergrift, Lindsey A., Wu, Shulin, Berker, Yannick, Habbel, Piet, Taupitz, Matthias, Wu, Chin-Lee & Cheng, Leo L. **Metabolomic prostate cancer fields in HRMAS MRS-profiled histologically benign tissue vary with cancer status and distance from cancer.** NMR in biomedicine 2019;32(10):e4038.

Berker, Yannick, Vandergrift, Lindsey A., Wagner, Isabel, Su, Li, Kurth, Johannes, Schuler, Andreas, Dinges, Sarah S., Habbel, Piet, Nowak, Johannes, Mark, Eugene, Aryee, Martin J., Christiani, David C. & Cheng, Leo L. **Magnetic Resonance Spectroscopy-based Metabolomic Biomarkers for Typing, Staging, and Survival Estimation of Early-Stage Human Lung Cancer.** Scientific reports 2019;9(1):10319.

Danksagung

Zu besonderem Dank bin ich meinem Doktorvater Herrn Prof. Dr. Matthias Taupitz für seinen wertvollen akademischen Rat und die zuverlässige Verfügbarkeit verpflichtet. Großen Dank spreche ich der Arbeitsgruppe aus, in der die präsentierte Arbeit durchgeführt wurde. Ich habe dort produktive Zusammenarbeit, inspirierende fachliche Diskussionen und außergewöhnliche Hilfbereitschaft erlebt habe. Insbesondere danke ich dabei Ass. Prof. Leo L. Cheng und Lindsey A. Vandergrift, die mich herzlich in Boston aufgenommen haben und stets die Begeisterung an dem Projekt geteilt haben. Für statistische Ratschläge und inhaltlichen Austausch danke ich herzlich Yannick Berker. Ich möchte außerdem Dr. Piet Habbel danken, ohne den das Projekt nicht zustande gekommen wäre und der mir fortwährend mit Rat und Tat zur Seite stand. Besonderer Dank möchte ich der Studienstiftung des Deutschen Volkes aussprechen, in den USA vertreten durch Dr. Lars Peters, deren finanzielle und ideelle Förderung maßgeblich zum Gelingen dieses Projektes beigetragen hat.

Außerdem möchte ich mich bei meiner Familie und Freunden bedanken. Ganz besonders danke ich meinen Eltern und Großeltern für die fortwährende liebevolle Unterstützung während meines gesamten Studiums und insbesondere während des Promotionsvorhabens.